



TECHNISCHE
UNIVERSITÄT
WIEN

Vienna University of Technology

DIPLOMARBEIT

Phonon laser linewidth near an exceptional point

ausgeführt am

Institut für Theoretische Physik
der Technischen Universität Wien

Institute for Theoretical Physics
Vienna University of Technology

unter der Anleitung von

Univ.Prof. Dipl.-Ing. Dr.techn. Stefan Rotter
Univ.Ass. Dr.rer.nat. Dmitry Krimer

durch

Kevin Pichler

Matrikelnummer 1025249

Hainburger Str. 66/22

1030 Wien, Österreich, EU

kevin.pichler@student.tuwien.ac.at

Wien, 12. September 2016

.....

Contents

Abstract	iii
1 Introduction	1
2 Theory	3
2.1 Phonon lasers	3
2.1.1 Concept	3
2.1.2 Experimental setup	4
2.1.3 Theoretical description	6
2.2 Laser linewidth	11
2.3 Exceptional Points	12
2.3.1 Influence on the laser linewidth	13
2.3.2 Exceptional points in phonon lasers	14
3 Methods	17
3.1 Numerical solution of stochastic differential equations	17
3.2 Linear stability analysis	22
3.3 Calculation of the signal linewidth	24
4 Results and Discussion	27
4.1 Phonon laser characteristics	28
4.1.1 Time-dependent solution of the system equations	28
4.1.2 Phonon laser threshold	32
4.1.3 Optomechanical amplification	35
4.2 Numerical linewidth calculations	37
4.2.1 Linewidth calculations for a conventional photon laser	37
4.2.2 Phonon laser linewidth calculations	39
5 Conclusions and Outlook	45
Acknowledgements	47
List of Figures and Tables	49
Bibliography	51

Abstract

The invention of the laser was certainly one of the most important technological developments of the 20th century. Countless laser applications in our daily life prove the significance of the process of stimulated emission of photons. Besides photons, however, also phonons can be amplified by stimulated emission. This gives rise to the concept of a phonon laser, which represents the sonic equivalent to an optical laser. In recent years, phonon lasers could even be realized experimentally.

While optical lasers have been used and studied for more than five decades, the theory of phonon lasers is much less developed. One of the missing links, for example, is a complete phonon laser linewidth theory. This thesis deals with the dependence of the phonon laser characteristics on various system and operating parameters. In particular, the behavior of the linewidth in the vicinity of an exceptional point is examined. Exceptional points occur when the eigenvalues and the corresponding eigenstates of a system coalesce. As we show on a theoretical level, such a non-Hermitian degeneracy results in nontrivial broadening of the phonon laser linewidth – a quantity that should also be accessible in the experiment.

1 Introduction

The impact of the laser on science and our daily life is tremendous. Although at first the laser was only of scientific interest, its enormous range of technological applications cannot be overestimated. Nowadays, lasers can be found nearly everywhere [1] – from barcode scanners in the supermarket through medical diagnostic and surgery tools to laser rangefinders – and usually we get in touch with laser applications on a daily basis. Moreover, countless industrial and scientific methods rely on the special properties of laser light [2], which is characterized by high intensity and coherence. The main principle behind laser operation is the process of *stimulated emission*.

Recently, it turned out that this principle can be applied not only to photons but also to phonons. Based on this understanding, the idea of a *phonon laser* was introduced [3,4]. Phonon lasers can be considered as the sonic equivalent to conventional photon lasers. Therefore, a phonon laser is often also called *SASER*, which is the acronym for *sound amplification by stimulated emission of radiation*. The idea of a coherent sound beam gives rise to promising possibilities of application [5]. Especially the high frequencies available (up to the THz range) make phonon lasers potentially useful, e.g. for high-resolution ultrasound imaging or probing and manipulating electronic devices at nanoscale level. However, phonon lasers are not yet ready for industrial applications, although a considerable number of successful experiments has been reported [6–8].

While optical lasers are well established in science and their characteristics are already described by a complete laser theory [9, 10], the relatively novel field of phonon lasers still leaves many unanswered questions. One of these open questions, for example, is the physical mechanism behind the phonon laser linewidth and its dependence on different system and operational parameters. In this context, also the influence of so-called *exceptional points* (EPs) on the system behavior is of enormous physical interest. At an EP, some of the eigenvalues and the corresponding eigenvectors of a system coalesce, which gives rise to novel features and fascinating new physics. Examples for the effects of EPs in lasers are the reversion of the pump dependence [11, 12] or the loss-induced suppression and revival of lasing [13]. Moreover, the laser linewidth was predicted to broaden in the vicinity of an EP. Therefore, it might be interesting to study the behavior of a phonon laser in connection with the influence of EPs as a first step into a new field of physics.

This thesis intends to study the properties of a phonon laser on a theoretical level. First, a set of dynamical system equations will be derived. With the help of this set of equations, several characteristic properties of the phonon laser will be investigated, as for example the dependence of the phonon laser threshold or amplification on various system and operating parameters. In particular, the linewidth of the phonon laser shall be calculated. The main focus of our studies will be the system behavior in the vicinity

of an exceptional point. The theoretical results will be compared to experimental data provided by the *Micro/Nano Photonics Lab* from *Washington University in St. Louis*.

2 Theory

2.1 Phonon lasers

2.1.1 Concept

In a nutshell, a laser consists of an active medium (gain medium), pumped by an external non-coherent source, and of a resonator. In optical lasers, the gain medium is often represented by an ensemble of atoms with different discrete energy levels. The pump mechanism excites the atoms into an upper energy level. If an excited electron drops to a lower energy level (e.g. to the ground state), the liberated energy (which is given by the difference between the binding energies of the two involved energy levels, $\Delta E = E_2 - E_1$) is emitted in form of a photon with frequency $\omega = \Delta E/\hbar$. Such a decay of an excited state with simultaneous emission of a photon can happen spontaneously or due to the interaction with another photon of the same frequency. The former process is called *spontaneous emission*, which occurs because of the limited lifetime of the excited state. The latter process (which is fundamental for a laser) is known as *stimulated emission* and was first discussed by Einstein in 1916 [14]. The principle of this process is schematically shown in [fig. 2.1](#). The crucial point about the stimulated emission is that the emitted photon has the same frequency, polarization, phase, and direction of travel as the incident photon. As a result, laser light is characterized by a high degree of coherence and high intensity due to constructive interference of the emitted photons. Photons can, however, also be absorbed by the atoms, causing a transition from the lower to the upper level. While stimulated emission leads to amplification, *absorption* causes the attenuation of light in the gain medium. Thus, it is important for the laser operation that the upper energy level is always more populated than the lower level (*population inversion*), which must be ensured by a sufficiently high pump power.

As a matter of fact, the principle of stimulated emission can be directly applied to *phonons* as well. Therefore, a phonon laser can be realized with any multi-state system where transitions between the energy levels are phonon mediated. In recent years, many different theoretical studies and successful experimental attempts to observe phonon laser action have been reported. Vahala *et al.* have realized a phonon laser where a single trapped ion interacts with a blue-detuned laser beam to coherently amplify phonons [6]. In contrast, the system of Beardsley *et al.* consists of a doped semiconductor superlattice with an electrical bias applied to it [7]. Another very different approach was presented by Grudinin *et al.* [8]. Their experiment, which is very similar to the system considered in this thesis (see [section 2.1.2](#)), makes use of the optomechanical interaction between two optical modes and one mechanical mode in a system of two coupled microresonators.

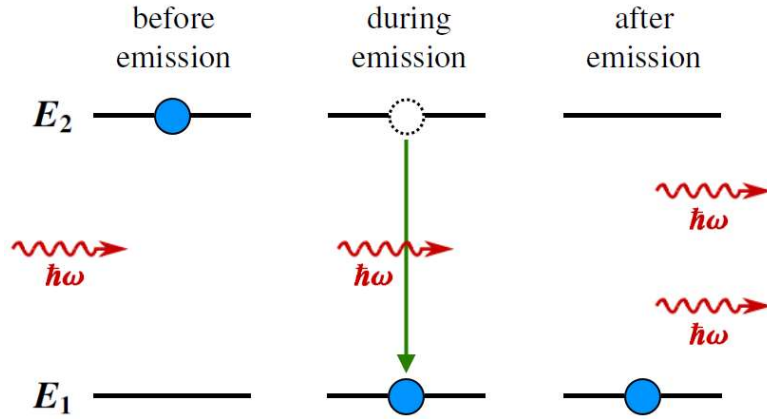


Figure 2.1: Principle of stimulated emission: the system with energy levels E_1 and E_2 is initially prepared in the upper level E_2 . Due to the interaction with an incident photon with energy $\hbar\omega = E_2 - E_1$, the system performs a transition from the upper to the lower energy level while emitting an additional photon with the same energy, phase, polarization, and direction as the incident photon.

Kabuss *et al.* have presented a scheme for the generation of coherent phonons by an optically driven semiconductor quantum dot coupled to an acoustic nanocavity [15, 16]. Note that an interaction between electromagnetic radiation and micromechanical motion is the central element in the field of *cavity optomechanics* [17]. The origin of this interaction lies in the radiation pressure forces induced through the momentum carried by light. Important for a phonon laser in this context is the possibility of *Raman scattering* [18, 19], a process which takes place due to the interaction between the light and the vibrations in an optomechanical cavity. One can distinguish here between *Stokes-* and *anti-Stokes-scattering*. In a Stokes-scattering process, a photon loses part of its energy which is transferred into the vibrational field by creating a phonon. If this process is stimulated by already existing phonons, then the phonons are coherently amplified and the system works as a phonon laser. In contrast, anti-Stokes-scattering means that a photon gains some energy which is taken from the vibrational field by annihilating a phonon. This effect can be used for cavity optomechanical cooling [20].

2.1.2 Experimental setup

In this thesis, we consider the system that was implemented in the *Micro/Nano Photonics Lab of Washington University in St. Louis* (see fig. 2.2). It consists of two coupled whispering gallery mode resonators (WGMRs)¹, similar to the system presented in [8]. The coupling between the two optical resonators is induced by the evanescent light field and the coupling strength is determined by the distance between the two discs. Energy is

¹ WGMRs consist of miniaturized dielectric structures having circular symmetry, which sustain electromagnetic waves that circulate within the structure. They are ideally suited for studying optomechanics as they combine ultra high finesse and Q-factors (corresponding to giant photon storage times) with microscale mode volume [21, 22].

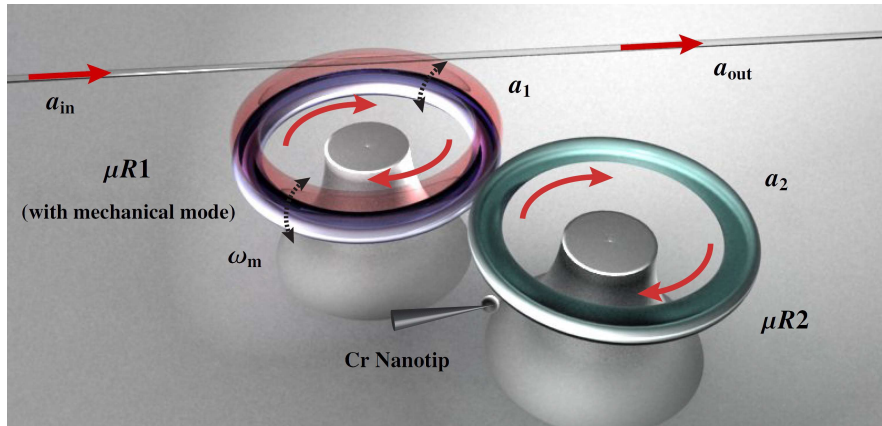


Figure 2.2: Phonon laser system considered in this thesis. The system consists of the two micro resonators $\mu R1$ and $\mu R2$ which contain the optical modes a_1 and a_2 . Furthermore, the first resonator supports a mechanical mode with resonance frequency ω_m . Additional loss can be introduced to the second resonator with a chromium nano-tip. The system is pumped via an optical fiber with input field a_{in} and output field a_{out} . Figure courtesy of Şahin Özdemir (Washington University in St. Louis)².

pumped into the system through a tapered optical fiber which is evanescently coupled to the first optical cavity. Additionally, the first resonator supports a mechanical mode which acts as the lasing mode in the system. In order to add some additional loss to the system, the second WGMR is coupled to a chromium nano-tip. The amount of additional loss is controlled by varying the distance between the tip and the edge of the WGMR. Without interaction, the two WGMRs have the same optical resonance frequency. However, due to the coupling of the two disks, the eigenmodes of the system are changed and a frequency splitting between the optical modes can be observed if the coupling constant is large compared to the optical dissipation rates. The resulting eigenmodes of the system are called *supermodes* [8]. A phonon laser can now be realized in two ways. The first possibility is to resonantly pump the optical supermode with the higher frequency. In this way, one gets an optical two-level system with a population inversion. Phonons are then coherently amplified by stimulated emission because of transitions between the two supermode levels. The frequency splitting between the two supermodes must be approximately equal to the mechanical resonance frequency. The second possibility to realize a phonon laser with this system is to non-resonantly pump one of the two supermodes where the difference between the pump frequency and the supermode frequency corresponds exactly to the mechanical resonance frequency. If the system is operating in this way, the respective supermode serves as the *Stokes-mode* in a *stimulated Raman scattering* process, similar to the case of a *Raman laser* [23]. The difference between the energy of the pump photons and the energy of the supermode photons is then available for the creation of a new phonon. The latter method is the one that was used in the actual experiment.

² Private communication, 2015.

2.1.3 Theoretical description

Hamiltonian

The system presented in [section 2.1.2](#) is theoretically described by the Hamiltonian

$$\hat{H} = \hat{H}_{\text{free}} + \hat{H}_{\text{int}} + \hat{H}_{\text{drive}}, \quad (2.1)$$

where \hat{H}_{free} is the free Hamiltonian of the uncoupled optical and mechanical modes, \hat{H}_{int} is the interaction part, and \hat{H}_{drive} represents the optical driving of the system. In our model, the optical and mechanical modes are represented by quantum harmonic oscillators. Therefore, the first part of [eq. \(2.1\)](#) is given by

$$\hat{H}_{\text{free}} = \hbar\omega_c \hat{a}_1^\dagger \hat{a}_1 + \hbar\omega_c \hat{a}_2^\dagger \hat{a}_2 + \hbar\omega_m \hat{b}^\dagger \hat{b}, \quad (2.2)$$

where ω_c is the resonance frequency of the (uncoupled) optical cavities and ω_m is the resonance frequency of the mechanical mode. The annihilation (creation) operators for the two optical modes and for the mechanical mode are denoted by $\hat{a}_{1,2}$ ($\hat{a}_{1,2}^\dagger$) and \hat{b} (\hat{b}^\dagger), respectively. Since both photons and phonons are *bosons*, their creation and annihilation operators satisfy the usual bosonic commutator relations

$$[\hat{m}, \hat{n}^\dagger] \equiv \hat{m}\hat{n}^\dagger - \hat{n}^\dagger\hat{m} = \delta_{mn}, \quad (2.3)$$

$$[\hat{m}, \hat{n}] = [\hat{m}^\dagger, \hat{n}^\dagger] = 0, \quad (2.4)$$

where δ_{mn} is the *Kronecker delta* and \hat{m} and \hat{n} can be any of the operators \hat{a}_1 , \hat{a}_2 , or \hat{b} . The interaction part in [eq. \(2.1\)](#) consists of the interaction between the two optical modes and the optomechanical interaction in the first cavity,

$$\hat{H}_{\text{int}} = \hat{H}_{\text{int}}^{(\text{opt})} + \hat{H}_{\text{int}}^{(\text{om})}. \quad (2.5)$$

The first term in [eq. \(2.5\)](#) depends on the inter-resonator coupling strength κ (coupling strength between the two optical modes) and is given by

$$\hat{H}_{\text{int}}^{(\text{opt})} = \hbar\kappa (\hat{a}_1^\dagger \hat{a}_2 + \hat{a}_2^\dagger \hat{a}_1). \quad (2.6)$$

The optomechanical interaction part in [eq. \(2.5\)](#) can be easily obtained by considering that the resonance frequency of the first cavity is modulated by the mechanical motion and hence is a function of the mechanical displacement x , which is given by the expectation value of the mechanical displacement operator $\hat{x} = x_0 (\hat{b} + \hat{b}^\dagger)$, where $x_0 = \sqrt{\hbar/(2m\omega_m)}$ is the zero-point fluctuation amplitude of the mechanical oscillator with effective mass m . A first order *Taylor series expansion* yields

$$\omega_c(x) \approx \omega_c + x \frac{\partial \omega_c}{\partial x} + \dots. \quad (2.7)$$

We can now define the optical frequency shift per displacement [\[17\]](#)

$$g := -\frac{\partial \omega_c}{\partial x}, \quad (2.8)$$

which directly leads to the optomechanical interaction Hamiltonian

$$\hat{H}_{\text{int}}^{(\text{om})} = -\hbar g x_0 \hat{a}_1^\dagger \hat{a}_1 (\hat{b} + \hat{b}^\dagger). \quad (2.9)$$

A more detailed derivation of the optomechanical interaction term is given in [24]. The total interaction Hamiltonian then reads

$$\hat{H}_{\text{int}} = \hbar \kappa (\hat{a}_1^\dagger \hat{a}_2 + \hat{a}_2^\dagger \hat{a}_1) - \hbar g x_0 \hat{a}_1^\dagger \hat{a}_1 (\hat{b} + \hat{b}^\dagger). \quad (2.10)$$

As the system is driven by a coherent continuous-wave laser, the last term in eq. (2.1) is given by

$$\hat{H}_{\text{drive}} = i\hbar (\Omega e^{-i\omega_d t} \hat{a}_1^\dagger - \text{H.c.}), \quad (2.11)$$

where Ω is the driving strength, ω_d is the driving frequency, and H.c. denotes the Hermitian conjugate. Combining the results of eqs. (2.2), (2.10) and (2.11) finally yields the complete system Hamiltonian

$$\begin{aligned} \hat{H} = & \hbar \omega_c (\hat{a}_1^\dagger \hat{a}_1 + \hat{a}_2^\dagger \hat{a}_2) + \hbar \omega_m \hat{b}^\dagger \hat{b} + \hbar \kappa (\hat{a}_1^\dagger \hat{a}_2 + \hat{a}_2^\dagger \hat{a}_1) \\ & - \hbar g x_0 \hat{a}_1^\dagger \hat{a}_1 (\hat{b} + \hat{b}^\dagger) + i\hbar (\Omega e^{-i\omega_d t} \hat{a}_1^\dagger - \text{H.c.}). \end{aligned} \quad (2.12)$$

For convenience, the optical modes are transformed to a frame rotating at the driving frequency ω_d , i.e. $\hat{a}_{1,2}^{\text{old}} = e^{-i\omega_d t} \hat{a}_{1,2}^{\text{new}}$. To this end, we apply the unitary transformation

$$\hat{U} = e^{i\omega_d t (\hat{a}_1^\dagger \hat{a}_1 + \hat{a}_2^\dagger \hat{a}_2)}, \quad (2.13)$$

which generates a new Hamiltonian with time-independent driving of the form

$$\begin{aligned} \hat{H} = & \hat{U} \hat{H}_{\text{old}} \hat{U}^\dagger - i\hbar \hat{U} \frac{\partial \hat{U}^\dagger}{\partial t} \\ = & -\hbar \Delta (\hat{a}_1^\dagger \hat{a}_1 + \hat{a}_2^\dagger \hat{a}_2) + \hbar \omega_m \hat{b}^\dagger \hat{b} + \hbar \kappa (\hat{a}_1^\dagger \hat{a}_2 + \hat{a}_2^\dagger \hat{a}_1) \\ & - \hbar g x_0 \hat{a}_1^\dagger \hat{a}_1 (\hat{b} + \hat{b}^\dagger) + i\hbar (\Omega \hat{a}_1^\dagger - \text{H.c.}), \end{aligned} \quad (2.14)$$

where $\Delta = \omega_d - \omega_c$ is the detuning between the driving laser frequency and the optical cavity resonance frequency.

Heisenberg equations of motion

Using the Hamiltonian eq. (2.14), we can derive the *Heisenberg equations of motion*, which can be written for an arbitrary operator \hat{o} according to

$$\frac{d}{dt} \hat{o} = \frac{i}{\hbar} [\hat{H}, \hat{o}]. \quad (2.15)$$

However, the Hamiltonian eq. (2.14) does not take into account the interaction of the system with a heat bath. These interactions are treated within the framework of input-

output theory [25, 26] and extend eq. (2.15) by adding terms standing for loss and quantum fluctuations,

$$\frac{d}{dt}\hat{\delta} = \frac{i}{\hbar} [\hat{H}, \hat{\delta}] - \gamma\hat{\delta} + \hat{\Gamma}, \quad (2.16)$$

where γ is the decay rate of the operator $\hat{\delta}$ and $\hat{\Gamma}$ is a statistical noise operator. The complete Heisenberg equations of motion for our system are then given by

$$\dot{\hat{a}}_1(t) = (i\Delta - \gamma_1)\hat{a}_1(t) - i\kappa\hat{a}_2(t) + igx_0\hat{a}_1(t)(\hat{b}(t) + \hat{b}^\dagger(t)) + \Omega + \hat{\Gamma}_1(t), \quad (2.17)$$

$$\dot{\hat{a}}_2(t) = (i\Delta - \gamma_2)\hat{a}_2(t) - i\kappa\hat{a}_1(t) + \hat{\Gamma}_2(t), \quad (2.18)$$

$$\dot{\hat{b}}(t) = (-i\omega_m - \gamma_m)\hat{b}(t) + igx_0\hat{a}_1^\dagger(t)\hat{a}_1(t) + \hat{\Gamma}_b(t), \quad (2.19)$$

in which $\gamma_{1,2}$ are the optical decay rates, γ_m is the mechanical decay rate, and $\hat{\Gamma}_{1,2}$ and $\hat{\Gamma}_b$ are the optical and mechanical noise operators. For the sake of completeness, we also present the set of eqs. (2.17) to (2.19) in terms of the mechanical displacement operator $\hat{x} = x_0(\hat{b} + \hat{b}^\dagger)$,

$$\dot{\hat{a}}_1(t) = (i\Delta - \gamma_1)\hat{a}_1(t) - i\kappa\hat{a}_2(t) + ig\hat{a}_1(t)\hat{x}(t) + \Omega + \hat{\Gamma}_1(t), \quad (2.20)$$

$$\dot{\hat{a}}_2(t) = (i\Delta - \gamma_2)\hat{a}_2(t) - i\kappa\hat{a}_1(t) + \hat{\Gamma}_2(t), \quad (2.21)$$

$$m\ddot{\hat{x}}(t) + m\gamma_m\dot{\hat{x}}(t) = -m\omega_m^2\hat{x}(t) + \hbar g\hat{a}_1^\dagger(t)\hat{a}_1(t) + \hat{\Gamma}_x(t), \quad (2.22)$$

where we have introduced the displacement noise operator $\hat{\Gamma}_x$.

The quantum noise in eqs. (2.17) to (2.19) is assumed to be *Markovian*³. Therefore, the noise operators are delta-correlated and satisfy the correlation relations [26]

$$\langle \hat{\Gamma}_1(t) \hat{\Gamma}_1^\dagger(t') \rangle = 2\gamma_1 (\bar{n}_{\text{th}}^{(\text{opt})} + 1) \delta(t - t'), \quad (2.23)$$

$$\langle \hat{\Gamma}_1^\dagger(t) \hat{\Gamma}_1(t') \rangle = 2\gamma_1 \bar{n}_{\text{th}}^{(\text{opt})} \delta(t - t'), \quad (2.24)$$

$$\langle \hat{\Gamma}_2(t) \hat{\Gamma}_2^\dagger(t') \rangle = 2\gamma_2 (\bar{n}_{\text{th}}^{(\text{opt})} + 1) \delta(t - t'), \quad (2.25)$$

$$\langle \hat{\Gamma}_2^\dagger(t) \hat{\Gamma}_2(t') \rangle = 2\gamma_2 \bar{n}_{\text{th}}^{(\text{opt})} \delta(t - t'), \quad (2.26)$$

$$\langle \hat{\Gamma}_b(t) \hat{\Gamma}_b^\dagger(t') \rangle = 2\gamma_m (\bar{n}_{\text{th}}^{(\text{mech})} + 1) \delta(t - t'), \quad (2.27)$$

$$\langle \hat{\Gamma}_b^\dagger(t) \hat{\Gamma}_b(t') \rangle = 2\gamma_m \bar{n}_{\text{th}}^{(\text{mech})} \delta(t - t'), \quad (2.28)$$

with the average number of thermally excited photons $\bar{n}_{\text{th}}^{(\text{opt})} \approx (e^{\hbar\omega_c/k_B T} - 1)^{-1}$ and the average number of thermally excited phonons $\bar{n}_{\text{th}}^{(\text{mech})} \approx (e^{\hbar\omega_m/k_B T} - 1)^{-1}$, where T is the environmental temperature and k_B is the Boltzmann constant. For all other combinations of the noise operators, the correlation functions vanish. In particular, the statistical

³ It is thus *memoryless*, i.e. the probability distribution of a future state does not depend on previous events but only on the current state.

averages of the quantum noise operators are all equal to zero,

$$\langle \hat{\Gamma}_1(t) \rangle = \langle \hat{\Gamma}_2(t) \rangle = \langle \hat{\Gamma}_b(t) \rangle = 0. \quad (2.29)$$

Note that the angle brackets in eqs. (2.23) to (2.29) mean a statistical average over many different noise realizations.

***c*-number Langevin equations**

Equations (2.17) to (2.19) represent a set of quantum operator Langevin equations. In order to solve these equations numerically and to simplify the analysis, the set of operator equations has to be transformed to a set of corresponding *c*-number equations, where the *c*-numbers are given by the expectation values of the respective operators. While *c*-numbers commute with each other, operators in general do not and therefore all operator products have to be preliminarily ordered. Specifically, one has to define a correspondence between a product of operators and a product of *c*-numbers. Here, we follow the procedure outlined in chapter 12 of [27] and choose the normal ordering $\hat{a}_1^\dagger, \hat{a}_2^\dagger, \hat{b}^\dagger, \hat{b}, \hat{a}_2, \hat{a}_1$. Since the system operators satisfy the commutator relations eqs. (2.3) and (2.4), the operator equations eqs. (2.17) to (2.19) are already in the chosen order and we can immediately write the *c*-number Langevin equations

$$\dot{a}_1(t) = (i\Delta - \gamma_1) a_1(t) - ika_2(t) + igx_0 a_1(t) (b(t) + b^*(t)) + \Omega + \Gamma_1(t), \quad (2.30)$$

$$\dot{a}_2(t) = (i\Delta - \gamma_2) a_2(t) - ika_1(t) + \Gamma_2(t), \quad (2.31)$$

$$\dot{b}(t) = (-i\omega_m - \gamma_m) b(t) + igx_0 a_1^*(t) a_1(t) + \Gamma_b(t). \quad (2.32)$$

The functions Γ in eqs. (2.30) to (2.32) are again the Langevin noise forces with the properties

$$\langle \Gamma_k(t) \rangle = 0, \quad (2.33)$$

$$\langle \Gamma_k(t) \Gamma_l(t') \rangle = D_{kl} \delta(t - t'), \quad (2.34)$$

$$\langle \Gamma_k^*(t) \Gamma_l(t') \rangle = D_{k^*l} \delta(t - t'), \quad (2.35)$$

where the indices k and l can be any of $\{1, 2, b\}$. The diffusion coefficients D_{kl} and D_{k^*l} , however, are not necessarily the same as those in eqs. (2.23) to (2.28) but have to be determined such that also the equations of motion for the second moments are identical to the corresponding normally ordered operator equations. As an example, we calculate the diffusion coefficient D_{1b} , which is defined by the relation

$$\langle \Gamma_1(t) \Gamma_b(t') \rangle = D_{1b} \delta(t - t'). \quad (2.36)$$

With the help of the operator equations of motion eqs. (2.17) and (2.19), we find that

$$\begin{aligned}
 \frac{d}{dt} \langle \hat{a}_1(t) \hat{b}(t) \rangle &= \langle \dot{\hat{a}}_1(t) \hat{b}(t) + \hat{a}_1(t) \dot{\hat{b}}(t) \rangle \\
 &= (i\Delta - \gamma_1) \langle \hat{a}_1 \hat{b} \rangle - i\kappa \langle \hat{a}_2 \hat{b} \rangle + igx_0 \langle \hat{a}_1 (\hat{b} + \hat{b}^\dagger) \hat{b} \rangle + \Omega \langle \hat{b} \rangle + \langle \hat{\Gamma}_1 \hat{b} \rangle \\
 &\quad + (-i\omega_m - \gamma_m) \langle \hat{a}_1 \hat{b} \rangle + igx_0 \langle \hat{a}_1 \hat{a}_1^\dagger \hat{a}_1 \rangle + \langle \hat{a}_1 \hat{\Gamma}_b \rangle \\
 &= (i\Delta - i\omega_m - \gamma_1 - \gamma_m) \langle \hat{a}_1 \hat{b} \rangle - i\kappa \langle \hat{a}_2 \hat{b} \rangle + igx_0 \langle \hat{a}_1 \hat{b} \hat{b} + \hat{a}_1 \hat{b}^\dagger \hat{b} \rangle \\
 &\quad + \Omega \langle \hat{b} \rangle + igx_0 \langle \hat{a}_1 \hat{a}_1^\dagger \hat{a}_1 \rangle + \langle \hat{\Gamma}_1 \hat{b} \rangle + \langle \hat{a}_1 \hat{\Gamma}_b \rangle. \tag{2.37}
 \end{aligned}$$

Evidently, the term $igx_0 \langle \hat{a}_1 \hat{a}_1^\dagger \hat{a}_1 \rangle$ is not in the chosen order. However, using the commutator relations eqs. (2.3) and (2.4), this term can be rewritten and brought into normal order according to

$$igx_0 \langle \hat{a}_1 \hat{a}_1^\dagger \hat{a}_1 \rangle = igx_0 \langle (\hat{a}_1^\dagger \hat{a}_1 + [\hat{a}_1, \hat{a}_1^\dagger]) \hat{a}_1 \rangle = igx_0 \langle \hat{a}_1^\dagger \hat{a}_1 \hat{a}_1 + \hat{a}_1 \rangle. \tag{2.38}$$

Furthermore, it can be shown that the system operators together with the corresponding noise operators satisfy the relation⁴ [28]

$$\langle \hat{\Gamma}_m(t) \hat{n}(t) \rangle + \langle \hat{m}(t) \hat{\Gamma}_n(t) \rangle = \hat{D}_{mn}, \tag{2.39}$$

in which \hat{m} and \hat{n} can be any of the system operators (\hat{a}_1 , \hat{a}_2 , or \hat{b}), $\hat{\Gamma}_m$ and $\hat{\Gamma}_n$ are the corresponding noise operators, and \hat{D}_{mn} denotes the diffusion coefficient on the operator level, which is defined by

$$\langle \hat{\Gamma}_m(t) \hat{\Gamma}_n(t') \rangle = \hat{D}_{mn} \delta(t - t'). \tag{2.40}$$

Therefore, the sum of the last two terms in eq. (2.37) can be replaced by the respective diffusion coefficient \hat{D}_{1b} , which is equal to zero,

$$\langle \hat{\Gamma}_1 \hat{b} \rangle + \langle \hat{a}_1 \hat{\Gamma}_b \rangle = \hat{D}_{1b} = 0. \tag{2.41}$$

Inserting the results of eqs. (2.38) and (2.41) into eq. (2.37) yields

$$\begin{aligned}
 \frac{d}{dt} \langle \hat{a}_1(t) \hat{b}(t) \rangle &= (i\Delta - i\omega_m - \gamma_1 - \gamma_m) \langle \hat{a}_1 \hat{b} \rangle - i\kappa \langle \hat{a}_2 \hat{b} \rangle \\
 &\quad + igx_0 \langle \hat{a}_1 \hat{b} \hat{b} + \hat{a}_1 \hat{b}^\dagger \hat{b} \rangle + \Omega \langle \hat{b} \rangle + igx_0 \langle \hat{a}_1^\dagger \hat{a}_1 \hat{a}_1 \rangle + igx_0 \langle \hat{a}_1 \rangle. \tag{2.42}
 \end{aligned}$$

⁴ An equivalent relation holds for the c -number quantities (a_1 , a_2 , and b) and the corresponding c -number noise forces (Γ_1 , Γ_2 , and Γ_b).

Now, we can perform the same calculation for the c -number quantities, where we use eqs. (2.30) and (2.32) and the fact that c -numbers commute with each other. The result is

$$\begin{aligned} \frac{d}{dt} \langle a_1(t) b(t) \rangle &= (i\Delta - i\omega_m - \gamma_1 - \gamma_m) \langle a_1 b \rangle - i\kappa \langle a_2 b \rangle \\ &+ igx_0 \langle a_1 b b + a_1 b^* b \rangle + \Omega \langle b \rangle + igx_0 \langle a_1^* a_1 a_1 \rangle + D_{1b}. \end{aligned} \quad (2.43)$$

By requiring the left-hand sides of eqs. (2.42) and (2.43) to be equal, the diffusion coefficient D_{1b} is found to be given by

$$D_{1b} = igx_0 \langle a_1 \rangle. \quad (2.44)$$

For our system, the diffusion coefficient D_{1b} is indeed the only one that differs from the corresponding operator diffusion coefficient. Consequently, the remaining non-vanishing c -number diffusion coefficients are given by

$$D_{1^*1} = 2\gamma_1 \bar{n}_{\text{th}}^{(\text{opt})}, \quad (2.45)$$

$$D_{2^*2} = 2\gamma_2 \bar{n}_{\text{th}}^{(\text{opt})}, \quad (2.46)$$

$$D_{b^*b} = 2\gamma_m \bar{n}_{\text{th}}^{(\text{mech})}. \quad (2.47)$$

In order to study the behavior of the phonon laser, eqs. (2.30) to (2.32) can be solved numerically, where it has to be ensured that the noise is implemented such that the relations for the diffusion coefficients eqs. (2.44) to (2.47) are satisfied. This procedure is explained in section 3.1 in more detail.

2.2 Laser linewidth

One of the most important properties of laser radiation is the intrinsic linewidth which arises because of quantum and thermal fluctuations. Even before the first laser was experimentally realized, Schawlow and Townes have found a fundamental limit for the laser linewidth which is given by the famous Schawlow-Townes formula [29]

$$\Delta\omega_{\text{ST}} = \frac{\hbar\omega_0\gamma_0^2}{2P}, \quad (2.48)$$

where ω_0 is the laser frequency, γ_0 is the passive cavity resonance width, and P is the output power of the laser. During the following decades, several multiplicative correction factors to the Schawlow-Townes formula have been introduced, leading to an improved linewidth formula of the form

$$\Delta\omega = \frac{\hbar\omega_0\tilde{\gamma}^2}{2P} \cdot n_{\text{sp}} \cdot (1 + \alpha^2) \cdot K. \quad (2.49)$$

The first correction is the *bad cavity factor* $\tilde{\gamma}$ [30], which arises if the gain linewidth γ_{\perp} is on the order of or smaller than the passive cavity resonance width γ_0 and causes

the substitution of γ_0 in eq. (2.48) with $\tilde{\gamma} = \frac{2\gamma_{\perp}\gamma_0}{2\gamma_{\perp}+\gamma_0}$. The second correction results from the incomplete inversion of the gain medium and is referred to as *spontaneous emission factor* $n_{\text{sp}} = \frac{N_2}{N_2-N_1}$ [31], where N_2 and N_1 are the spatially averaged populations in the upper and lower states of the lasing transition. Another modification of the linewidth is given by the *Henry α factor* [32], which is caused by the nonlinear coupling between the amplitude and phase fluctuations of the laser field. Finally, the laser linewidth is enhanced by the *Petermann factor* K [33]. Due to the presence of the gain medium as well as the openness of the laser cavity, the modes are not power-orthogonal, which results in an enhancement of the noise power [34–36]. Such behavior has also been experimentally verified [37, 38].

The correction factors in eq. (2.49) have been derived under certain approximations and do not fully consider the space-dependence of the electric fields or nonlinear effects like *spatial hole-burning*. In recent years, a linewidth theory which also takes such effects into account has been proposed [39–41]. This theory is based on the *steady-state ab initio laser theory* (SALT) [42, 43]. However, the equations of our phonon laser system eqs. (2.30) to (2.32) have a different structure as the conventional laser equations treated in the framework of SALT. Therefore, SALT is not directly applicable and the phonon laser linewidth has to be calculated numerically as described in section 3.3.

2.3 Exceptional Points

An important influence on the behavior of lasers is given by the possibility of inducing so-called exceptional points. The term *exceptional point* (EP) has been introduced by Kato [44] and it refers to a special property of non-Hermitian matrices [45–47]. As opposed to common Hermitian degeneracies, an EP occurs when not only some of the eigenvalues of a system but also the corresponding eigenvectors coalesce. As an example, let us consider the following non-Hermitian 2×2 matrix

$$M = \begin{pmatrix} a - ib & \kappa \\ \kappa & c - id \end{pmatrix} \quad (2.50)$$

with real parameters a , b , c , d , and κ . By varying these parameters, one can now induce an EP in the matrix M . Here we keep a , b , and c constant, e.g. $a = b = c = 1$, and vary the parameters d and κ . The behavior of the eigenvalues for this situation is illustrated in fig. 2.3. Obviously, the eigenvalue sheets can be divided into two regions – one region where the real parts of the two eigenvalues are equal and the imaginary parts differ and another region where the real parts differ and the imaginary parts are equal. The feature along the border between these regions, where both real and imaginary parts of the eigenvalues are equal, could be called an *exceptional line*. Thus, it is possible to induce an EP for any given value of κ by varying the parameter d , which is very similar to the procedure followed in the experiment as described in section 2.3.2.

The appearance of EPs leads to many interesting phenomena in a wide range of physical problems. EPs can have drastic effects in the above-threshold behavior of

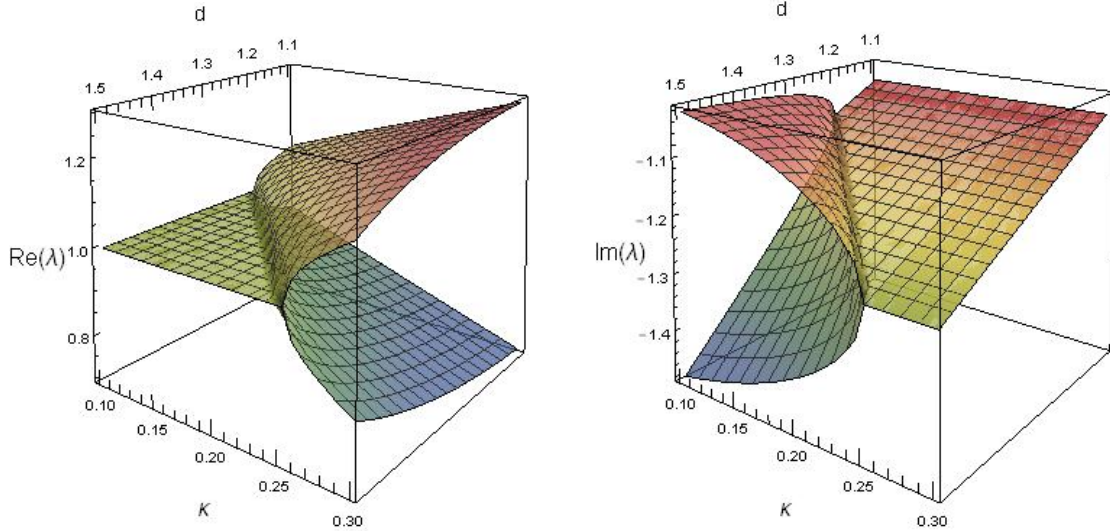


Figure 2.3: Eigenvalues of the non-Hermitian matrix M (eq. (2.50)) as a function of d and κ for constant parameters $a = b = c = 1$. The left picture shows the real part and the right picture shows the imaginary part of the two eigenvalues λ .

lasers, as for instance a counter-intuitive laser turn-off although the overall pump power deposited in the system is increased [11, 12] or the opposite effect of switching on although the total loss of the system is increased [13]. Another example for the influence of EPs is the state-switching in a system of coupled oscillator modes caused by an adiabatic encircling of an EP [48, 49]. Furthermore, the influence of EPs on *parity-time-symmetric* (\mathcal{PT} -symmetric) systems is of special interest [50]. It was shown that also a non-Hermitian Hamiltonian can have an entirely real spectrum if the system satisfies the condition of \mathcal{PT} -symmetry [51]. A symmetry-breaking, where the eigenvalues become complex, is always connected with the occurrence of an EP in the system [52–55].

2.3.1 Influence on the laser linewidth

The influence of EPs on the laser linewidth is subject of enormous physical interest. The closer a system is steered towards an EP, the more its eigenmodes approach each other. In other words, the eigenmodes become more and more non-orthogonal in the vicinity of an EP. According to the Petermann-theory (see section 2.2), this leads to an additional linewidth enhancement which should reach its maximum exactly at the EP [56]. Although there exist experiments where exceptional points have been induced in lasers (see e.g. [12, 13]), the linewidth broadening behavior in the vicinity of the EP could not be experimentally verified. The reason for that is that the currently available spectrum analyzers cannot resolve the laser linewidth for the relevant laser frequencies ($\sim 10^{12} - 10^{15}$ Hz). The linewidth of mechanical oscillations with MHz to THz frequencies, however, can be measured more precisely. Therefore, it would be desirable to investigate the phonon laser linewidth at an EP. However, the EP in our system does not concern the mechanical mode but only the optical modes, as outlined

in [section 2.3.2](#). The situation is thus more complicated than in an optical laser and the Petermann-theory is not directly applicable. Nevertheless, the influence of EPs leads to interesting features as it is shown in [chapter 4](#).

2.3.2 Exceptional points in phonon lasers

In our phonon laser system, only one mechanical mode is excited. Thus, the EP cannot be induced in the mechanical part of the system but rather in the optical part, which contains two optical modes. This can be achieved by varying several system parameters. If we take a look on [eqs. \(2.17\)](#) and [\(2.18\)](#) and ignore the optomechanical interaction, we can write down the equations for the two coupled optical modes alone,

$$\dot{\hat{a}}_1(t) = (i\Delta - \gamma_1) \hat{a}_1(t) - i\kappa \hat{a}_2(t) + \Omega + \hat{\Gamma}_1(t), \quad (2.51)$$

$$\dot{\hat{a}}_2(t) = (i\Delta - \gamma_2) \hat{a}_2(t) - i\kappa \hat{a}_1(t) + \hat{\Gamma}_2(t). \quad (2.52)$$

[Equations \(2.51\)](#) and [\(2.52\)](#) can be reformulated as a matrix equation,

$$\frac{d}{dt} \begin{pmatrix} \hat{a}_1(t) \\ \hat{a}_2(t) \end{pmatrix} = -i \underbrace{\begin{pmatrix} -\Delta - i\gamma_1 & \kappa \\ \kappa & -\Delta - i\gamma_2 \end{pmatrix}}_M \begin{pmatrix} \hat{a}_1(t) \\ \hat{a}_2(t) \end{pmatrix} + \begin{pmatrix} \Omega + \hat{\Gamma}_1(t) \\ \hat{\Gamma}_2(t) \end{pmatrix}. \quad (2.53)$$

The eigenvalues of this system can be found by solving the characteristic equation

$$|M - \lambda \mathbb{1}| = \begin{vmatrix} -\Delta - i\gamma_1 - \lambda & \kappa \\ \kappa & -\Delta - i\gamma_2 - \lambda \end{vmatrix} = 0, \quad (2.54)$$

which leads to the solutions for the complex supermode frequencies

$$\lambda_{\pm} = -\Delta - i\frac{\gamma_1 + \gamma_2}{2} \pm \sqrt{\kappa^2 - \frac{(\gamma_2 - \gamma_1)^2}{4}}. \quad (2.55)$$

The corresponding eigenvectors (supermodes) are defined by the equation

$$(M - \lambda_{\pm} \mathbb{1}) \mathbf{v}_{\pm} = \mathbf{0} \quad (2.56)$$

and the solutions read

$$\mathbf{v}_{\pm} = \frac{1}{N_{\pm}} \begin{pmatrix} i(\gamma_2 - \gamma_1) \mp \sqrt{4\kappa^2 - (\gamma_2 - \gamma_1)^2} \\ 2\kappa \end{pmatrix}, \quad (2.57)$$

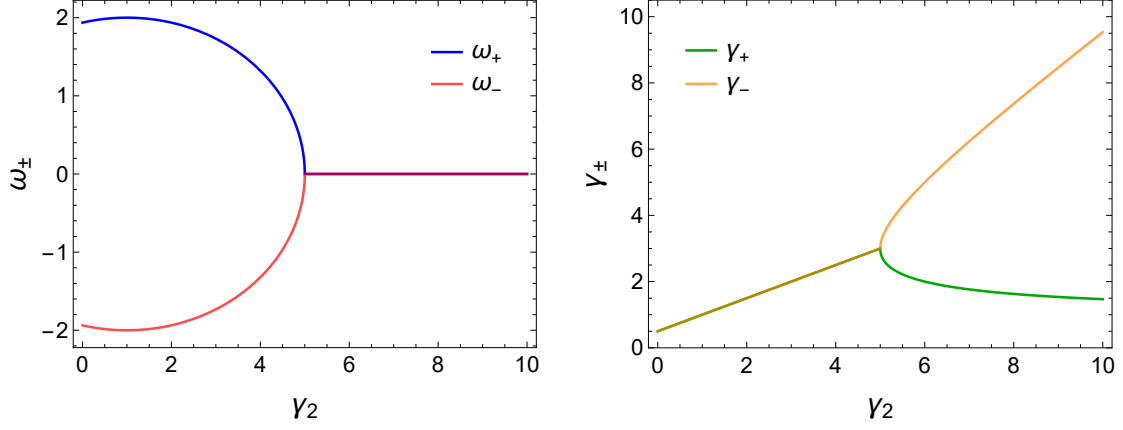


Figure 2.4: Frequencies $\omega_{\pm} = \text{Re}(\lambda_{\pm})$ (left) and dissipation rates $\gamma_{\pm} = -\text{Im}(\lambda_{\pm})$ (right) of the supermodes \hat{a}_{\pm} as a function of γ_2 . For simplicity, we chose the dimensionless parameters $\Delta = 0$, $\kappa = 2$, and $\gamma_1 = 1$.

with the normalization constants

$$N_{\pm} = \begin{cases} \sqrt{8} \kappa & \text{if } [4\kappa^2 - (\gamma_2 - \gamma_1)^2] \geq 0 \\ \sqrt{4\kappa^2 + \left(\gamma_2 - \gamma_1 \mp \sqrt{(\gamma_2 - \gamma_1)^2 - 4\kappa^2}\right)^2} & \text{if } [4\kappa^2 - (\gamma_2 - \gamma_1)^2] < 0 \end{cases} \quad (2.58)$$

Therefore, the supermodes are given by linear combinations of the cavity modes \hat{a}_1 and \hat{a}_2 ,

$$\hat{a}_{\pm}(t) = \frac{1}{N_{\pm}} \left[\left(i(\gamma_2 - \gamma_1) \mp \sqrt{4\kappa^2 - (\gamma_2 - \gamma_1)^2} \right) \hat{a}_1(t) + 2\kappa \hat{a}_2(t) \right]. \quad (2.59)$$

The real parts of the complex supermode frequencies [eq. \(2.55\)](#) represent the new supermode resonant frequencies $\omega_{\pm} = \text{Re}(\lambda_{\pm})$ and the negative imaginary parts are the corresponding dissipation rates $\gamma_{\pm} = -\text{Im}(\lambda_{\pm})$. If the term under the square root in [eqs. \(2.55\)](#) and [\(2.59\)](#) vanishes, i.e. if $4\kappa^2 = (\gamma_2 - \gamma_1)^2$, then the two eigenvalues as well as the corresponding eigenvectors coalesce. This situation defines the EP. Therefore, an EP can be induced by controlling the parameters κ , γ_1 , and γ_2 . In our system, the loss in the second WGMR is modified by adding extra loss through the tip, i.e. $\gamma_2 \rightarrow \gamma_{2,0} + \gamma_{\text{tip}}$, where $\gamma_{2,0}$ is the intrinsic loss of the second WGMR and γ_{tip} is the loss induced by the tip. The values of γ_1 and κ were kept constant in the experiment. [Figure 2.4](#) shows the typical behavior of the supermode frequencies and dissipation rates in the vicinity of an EP.

Finally, it should be recalled that the EP only applies to the optical part of the system. Thus, there is no EP regarding the (lasing) mechanical mode. Consequently, we have a different situation as in [\[12, 13\]](#), where the EP directly concerned the lasing modes.

3 Methods

3.1 Numerical solution of stochastic differential equations

Over the years, a huge variety of methods for the solution of differential equations has been developed. The common methods which are valid for the solution of *ordinary* differential equations (ODEs), however, are not directly applicable to *stochastic* differential equations (SDEs). SDEs are equations of the form

$$\frac{d}{dt}x(t) = f(x(t), t, \xi(t)) , \quad (3.1)$$

where f is an arbitrary function of the variable $x(t)$ itself, the time t , and a stochastic process $\xi(t)$. For our purposes, it is sufficient to reduce the considerations to a simpler form of equations,

$$\frac{d}{dt}x(t) = f(x(t)) + \xi(t) , \quad (3.2)$$

where the function f only depends on the variable x and the stochastic process appears in the form of an additive noise term⁵. The stochastic process $\xi(t)$ is assumed to be a *Gaussian white noise* with the properties

$$\langle \xi(t) \rangle = 0 , \quad (3.3)$$

$$\langle \xi(t) \xi(t') \rangle = D \delta(t - t') , \quad (3.4)$$

where the diffusion coefficient D determines the noise strength. *Gaussian* means that the values of the noise term follow a normal distribution with zero mean and variance D . The white noise is a non-analytic function and can be defined as the derivative of a special stochastic process, namely the *Wiener process* $W(t)$ ⁶,

$$\xi(t) = \frac{d}{dt}W(t) . \quad (3.5)$$

Examples for typical realizations of a Wiener process are shown in [fig. 3.1](#).

As in numerical calculations time takes always discrete values, we aim to write the

⁵ For simplicity, all quantities are assumed to be real at this point. However, the concept can be easily transferred to complex numbers.

⁶ The Wiener process is a continuous-time stochastic process which is, for example, used to describe *Brownian motion*. It can be interpreted as the continuous limit of a one-dimensional random walk.

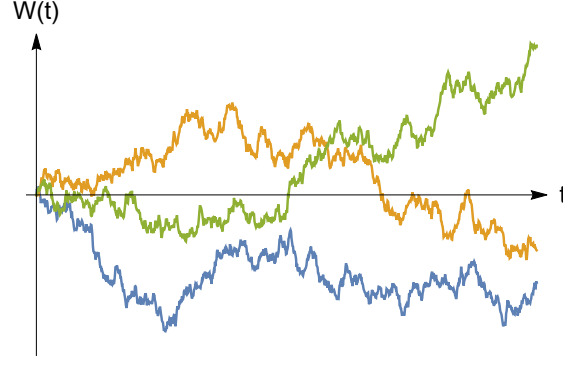


Figure 3.1: Three different trajectories of a Wiener process $W(t)$.

formal solution of eq. (3.2) for one time step h ,

$$x(t+h) = x(t) + \underbrace{\int_t^{t+h} f(x(s)) ds}_{F_h(t)} + \underbrace{\int_t^{t+h} \xi(s) ds}_{w_h(t)}, \quad (3.6)$$

in which the integral is separated into a deterministic part $F_h(t)$ and a stochastic contribution $w_h(t)$. The deterministic part can be calculated using any common method for integrating ODEs. The stochastic contribution, however, needs a special treatment. Using eq. (3.5), $w_h(t)$ can be expressed as the difference of the Wiener process at two different times,

$$w_h(t) = W(t+h) - W(t). \quad (3.7)$$

Therefore, $w_h(t)$ is a Gaussian process characterized by the properties

$$\langle w_h(t) \rangle = \int_t^{t+h} \langle \xi(s) \rangle ds = 0, \quad (3.8)$$

$$\langle w_h(t) w_h(t') \rangle = \int_t^{t+h} \int_{t'}^{t'+h} \langle \xi(s) \xi(u) \rangle ds du = \int_t^{t+h} \int_{t'}^{t'+h} D \delta(s-u) ds du, \quad (3.9)$$

which follows directly from eqs. (3.3) and (3.4). In order to evaluate the integral in eq. (3.9), we assume, without loss of generality, that $t' > t$. If $t' > t+h$, the delta function vanishes as there is no overlap in the integration intervals and the integral is equal to zero. For $t \leq t' < t+h$, the result is

$$\langle w_h(t) w_h(t') \rangle = \int_{t'}^{t+h} D ds = D(t-t'+h). \quad (3.10)$$

By considering discrete times $t = t_i = ih$ and $t' = t_j = jh$, the correlation becomes

$$\langle w_h(t_i) w_h(t_j) \rangle = Dh \delta_{ij}. \quad (3.11)$$

For the numerical implementation of $w_h(t_i)$, we introduce a set of independent Gaussian random numbers $\{r_i\}$ with zero mean and variance 1,

$$\langle r_i \rangle = 0, \quad (3.12)$$

$$\langle r_i r_j \rangle = \delta_{ij}. \quad (3.13)$$

The stochastic contribution $w_h(t_i)$ is then given by

$$w_h(t_i) = \sqrt{Dh} r_i, \quad (3.14)$$

and hence the solution for $x(t)$ with the initial value x_0 can be generated according to

$$x(t_0) = x_0, \quad (3.15)$$

$$x(t_{i+1}) = x(t_i) + F_h(t_i) + \sqrt{Dh} r_i. \quad (3.16)$$

In this way, we have found a recurrence relation for the solution of SDEs of the form [eq. \(3.2\)](#). A more detailed treatment of stochastic differential equations can be found in [\[57, 58\]](#).

We are now in the position to apply the above considerations to our case of a phonon laser. In [section 2.1.3](#), we have derived the c -number equations ([eqs. \(2.30\) to \(2.32\)](#)) which describe our phonon laser system. These equations represent a set of coupled Langevin equations, i.e. they are stochastic differential equations of the form

$$\frac{d}{dt} \mathbf{x}(t) = \mathbf{f}(\mathbf{x}(t)) + \boldsymbol{\xi}(t), \quad (3.17)$$

in which \mathbf{f} is a function of the variables $\mathbf{x} = (a_1, a_2, b)$ and $\boldsymbol{\xi} = (\Gamma_1, \Gamma_2, \Gamma_b)$ is a vector of Gaussian white noises. Similarly as before, [eq. \(3.17\)](#) can be split into the deterministic part \mathbf{f} and the stochastic contribution $\boldsymbol{\xi}$. The deterministic part is solved with the *fourth-order Runge-Kutta method* [\[59\]](#). While simpler methods only take into account the function \mathbf{f} at the beginning of the time interval for the computation of one time step, the Runge-Kutta method also uses intermediate time steps, which results in higher accuracy and convergence. After the calculation of the deterministic part, the noise term $\mathbf{w}_h(t_i) = \sqrt{h} \mathbf{n}_i$ has to be added, in accordance with [eq. \(3.16\)](#). Each time step of the numerical integration is then computed with the following algorithm:

$$\mathbf{k}_1 = \mathbf{f}(\mathbf{x}_i), \quad (3.18)$$

$$\mathbf{k}_2 = \mathbf{f}(\mathbf{x}_i + \frac{h}{2} \mathbf{k}_1), \quad (3.19)$$

$$\mathbf{k}_3 = \mathbf{f}(\mathbf{x}_i + \frac{h}{2} \mathbf{k}_2), \quad (3.20)$$

$$\mathbf{k}_4 = \mathbf{f}(\mathbf{x}_i + h \mathbf{k}_3), \quad (3.21)$$

$$\mathbf{x}_{i+1} = \mathbf{x}_i + \frac{h}{6} (\mathbf{k}_1 + 2\mathbf{k}_2 + 2\mathbf{k}_3 + \mathbf{k}_4) + \sqrt{h} \mathbf{n}_i. \quad (3.22)$$

In the remaining part of this section, we concentrate on the appropriate implementation

of the noise term \mathbf{n}_i . The fields a_1 , a_2 , and b , as well as the corresponding noise forces in eqs. (2.30) to (2.32) are complex-valued functions. Consequently, the noise term \mathbf{n}_i is also complex-valued and can therefore be split into a real and an imaginary part,

$$\mathbf{n} = \begin{pmatrix} n_1 \\ n_2 \\ n_b \end{pmatrix} = \begin{pmatrix} n_1^{\text{Re}} + i n_1^{\text{Im}} \\ n_2^{\text{Re}} + i n_2^{\text{Im}} \\ n_b^{\text{Re}} + i n_b^{\text{Im}} \end{pmatrix} = \begin{pmatrix} \alpha_1 r_1^\alpha + i \beta_1 r_1^\beta \\ \alpha_2 r_2^\alpha + i \beta_2 r_2^\beta \\ \alpha_b r_b^\alpha + i \beta_b r_b^\beta \end{pmatrix}, \quad (3.23)$$

where we have dropped the index i for simplicity and to avoid confusion with the imaginary unit. Both real and imaginary parts are presented as a product of a certain prefactor (α_k, β_k) and a Gaussian random number (r_k^α, r_k^β) with zero mean and variance 1. Combining the result eq. (3.11) with the non-vanishing diffusion coefficients eqs. (2.44) to (2.47) yields the following constraints for the noise terms,

$$\langle n_1^* n_1 \rangle = D_{1^*1}, \quad (3.24)$$

$$\langle n_2^* n_2 \rangle = D_{2^*2}, \quad (3.25)$$

$$\langle n_b^* n_b \rangle = D_{b^*b}, \quad (3.26)$$

$$\langle n_1 n_b \rangle = D_{1b}, \quad (3.27)$$

where the correlations for all other combinations of the noise terms are equal to zero. The next step is to determine the constants α_k and β_k . For each of the n_k , we can write

$$\langle n_k^* n_k \rangle = \langle (\alpha_k r_k^\alpha - i \beta_k r_k^\beta) (\alpha_k r_k^\alpha + i \beta_k r_k^\beta) \rangle = \alpha_k^2 \underbrace{\langle r_k^\alpha r_k^\alpha \rangle}_1 + \beta_k^2 \underbrace{\langle r_k^\beta r_k^\beta \rangle}_1 = D_{k^*k} \quad (3.28)$$

$$\implies \alpha_k^2 + \beta_k^2 = D_{k^*k} \quad (3.29)$$

and

$$\langle n_k n_k \rangle = \langle (\alpha_k r_k^\alpha + i \beta_k r_k^\beta)^2 \rangle = \alpha_k^2 \underbrace{\langle r_k^\alpha r_k^\alpha \rangle}_1 - \beta_k^2 \underbrace{\langle r_k^\beta r_k^\beta \rangle}_1 + 2i \alpha_k \beta_k \underbrace{\langle r_k^\alpha r_k^\beta \rangle}_0 = 0 \quad (3.30)$$

$$\implies \alpha_k^2 = \beta_k^2. \quad (3.31)$$

Inserting eq. (3.31) into eq. (3.29), one finds that

$$\alpha_k^2 = \beta_k^2 = \frac{1}{2} D_{k^*k} \quad (3.32)$$

and therefore

$$\alpha_1 = \beta_1 = \sqrt{\gamma_1 \bar{n}_{\text{th}}^{(\text{opt})}}, \quad (3.33)$$

$$\alpha_2 = \beta_2 = \sqrt{\gamma_2 \bar{n}_{\text{th}}^{(\text{opt})}}, \quad (3.34)$$

$$\alpha_b = \beta_b = \sqrt{\gamma_m \bar{n}_{\text{th}}^{(\text{mech})}}. \quad (3.35)$$

Hitherto, we have considered exclusively the constraints given by eqs. (3.24) to (3.26), so we still have to fulfill the last constraint eq. (3.27). At first glance, the noise terms seem to be overdetermined. However, it is possible to introduce specific correlations between certain random numbers such that all conditions are simultaneously satisfied. To this end, we write the correlation

$$\begin{aligned} \langle n_1^* n_b \rangle &= \langle (\alpha_1 r_1^\alpha - i \beta_1 r_1^\beta) (\alpha_b r_b^\alpha + i \beta_b r_b^\beta) \rangle \\ &= \sqrt{\gamma_1 \gamma_m \bar{n}_{\text{th}}^{(\text{opt})} \bar{n}_{\text{th}}^{(\text{mech})}} \left[\langle r_1^\alpha r_b^\alpha \rangle + \langle r_1^\beta r_b^\beta \rangle + i \left(\langle r_1^\alpha r_b^\beta \rangle - \langle r_1^\beta r_b^\alpha \rangle \right) \right] = 0, \end{aligned} \quad (3.36)$$

where we used the relation

$$\alpha_1 \alpha_b = \beta_1 \beta_b = \alpha_1 \beta_b = \beta_1 \alpha_b = \sqrt{\gamma_1 \gamma_m \bar{n}_{\text{th}}^{(\text{opt})} \bar{n}_{\text{th}}^{(\text{mech})}}. \quad (3.37)$$

Equation (3.36) implies that

$$\langle r_1^\alpha r_b^\alpha \rangle = - \langle r_1^\beta r_b^\beta \rangle, \quad (3.38)$$

$$\langle r_1^\alpha r_b^\beta \rangle = \langle r_1^\beta r_b^\alpha \rangle. \quad (3.39)$$

With the help of eqs. (3.38) and (3.39), we can write the other correlation

$$\begin{aligned} \langle n_1 n_b \rangle &= \langle (\alpha_1 r_1^\alpha + i \beta_1 r_1^\beta) (\alpha_b r_b^\alpha + i \beta_b r_b^\beta) \rangle \\ &= \sqrt{\gamma_1 \gamma_m \bar{n}_{\text{th}}^{(\text{opt})} \bar{n}_{\text{th}}^{(\text{mech})}} \left[\langle r_1^\alpha r_b^\alpha \rangle - \langle r_1^\beta r_b^\beta \rangle + i \left(\langle r_1^\alpha r_b^\beta \rangle + \langle r_1^\beta r_b^\alpha \rangle \right) \right] \\ &= \sqrt{\gamma_1 \gamma_m \bar{n}_{\text{th}}^{(\text{opt})} \bar{n}_{\text{th}}^{(\text{mech})}} 2 \left(\langle r_1^\alpha r_b^\alpha \rangle + i \langle r_1^\alpha r_b^\beta \rangle \right) = D_{1b} = igx_0 \langle a_1 \rangle. \end{aligned} \quad (3.40)$$

Therefore, all constraints for the noise terms can be satisfied if the random numbers meet the additional requirements

$$- \langle r_1^\alpha r_b^\alpha \rangle = \langle r_1^\beta r_b^\beta \rangle = \frac{gx_0}{2 \sqrt{\gamma_1 \gamma_m \bar{n}_{\text{th}}^{(\text{opt})} \bar{n}_{\text{th}}^{(\text{mech})}}} \text{Im}(\langle a_1 \rangle), \quad (3.41)$$

$$\langle r_1^\alpha r_b^\beta \rangle = \langle r_1^\beta r_b^\alpha \rangle = \frac{gx_0}{2 \sqrt{\gamma_1 \gamma_m \bar{n}_{\text{th}}^{(\text{opt})} \bar{n}_{\text{th}}^{(\text{mech})}}} \text{Re}(\langle a_1 \rangle). \quad (3.42)$$

One possibility to fulfill the correlations eqs. (3.41) and (3.42) is to specifically replace the random numbers r_b^α and r_b^β for a certain number of noise realizations by the random numbers r_1^α and r_1^β . For a sufficiently large number of different noise realizations N , we can write for $i \neq j$

$$\langle r_i r_j \rangle = \frac{1}{N} \sum_{\mu=1}^N r_i^\mu r_j^\mu = 0, \quad (3.43)$$

$$\langle r_i r_i \rangle = \frac{1}{N} \sum_{\mu=1}^N r_i^\mu r_i^\mu = 1, \quad (3.44)$$

and therefore with $0 \ll M < N$

$$\langle r_i r_j \rangle_M := \frac{1}{N} \left(\sum_{\mu=1}^M r_i^\mu r_j^\mu + \sum_{\mu=M+1}^N r_i^\mu r_j^\mu \right) = \frac{M}{N}. \quad (3.45)$$

Hence, we can satisfy the conditions eqs. (3.41) and (3.42) for a total number of N noise realizations with $L + M \leq N$ if we make L times the replacements

$$r_b^\alpha \rightarrow -\text{sgn}[\text{Im}(\langle a_1 \rangle)] r_1^\alpha, \quad (3.46)$$

$$r_b^\beta \rightarrow \text{sgn}[\text{Im}(\langle a_1 \rangle)] r_1^\beta, \quad (3.47)$$

and M times the replacements

$$r_b^\alpha \rightarrow \text{sgn}[\text{Re}(\langle a_1 \rangle)] r_1^\beta, \quad (3.48)$$

$$r_b^\beta \rightarrow \text{sgn}[\text{Re}(\langle a_1 \rangle)] r_1^\alpha, \quad (3.49)$$

where sgn is the sign function and L and M are determined by the relations

$$\frac{L}{N} = \frac{g x_0}{2 \sqrt{\gamma_1 \gamma_m \bar{n}_{\text{th}}^{(\text{opt})} \bar{n}_{\text{th}}^{(\text{mech})}}} |\text{Im}(\langle a_1 \rangle)|, \quad (3.50)$$

$$\frac{M}{N} = \frac{g x_0}{2 \sqrt{\gamma_1 \gamma_m \bar{n}_{\text{th}}^{(\text{opt})} \bar{n}_{\text{th}}^{(\text{mech})}}} |\text{Re}(\langle a_1 \rangle)|. \quad (3.51)$$

Obviously, this method is valid only if

$$\frac{g x_0}{2 \sqrt{\gamma_1 \gamma_m \bar{n}_{\text{th}}^{(\text{opt})} \bar{n}_{\text{th}}^{(\text{mech})}}} (|\text{Re}(\langle a_1 \rangle)| + |\text{Im}(\langle a_1 \rangle)|) \leq 1, \quad (3.52)$$

which is always fulfilled with the parameters that were used for the calculations presented in [chapter 4](#).

3.2 Linear stability analysis

For numerous issues of our phonon laser system, it is necessary to know the lasing threshold pump power. A standard way to find the laser threshold is given by a technique called *linear stability analysis* [60]. A particular solution of a non-linear system is called *linearly stable* if the linearization of the equations at this solution is of the form

$$\frac{d}{dt} \mathbf{u}(t) = \mathbf{A} \mathbf{u}(t), \quad (3.53)$$

where the spectrum of the linear operator \mathbf{A} contains only eigenvalues with negative real part. Otherwise, if one of the eigenvalues has a positive real part, the system is

called *linearly unstable*. For our system of a phonon laser, the transition between linear stability and instability corresponds to the laser threshold. In order to linearize the system equations, the fields $a_1(t)$, $a_2(t)$, and $b(t)$ are split into a constant steady-state value and a small time-dependent perturbation⁷, i.e.

$$a_1(t) \rightarrow \bar{a}_1 + \delta a_1(t), \quad (3.54)$$

$$a_2(t) \rightarrow \bar{a}_2 + \delta a_2(t), \quad (3.55)$$

$$b(t) \rightarrow \bar{b} + \delta b(t). \quad (3.56)$$

Inserting eqs. (3.54) to (3.56) into eqs. (2.30) to (2.32) yields the linearized equations

$$\begin{aligned} \frac{d}{dt} (\bar{a}_1 + \delta a_1(t)) &= (i\Delta - \gamma_1) (\bar{a}_1 + \delta a_1(t)) - i\kappa (\bar{a}_2 + \delta a_2(t)) + \Omega \\ &\quad + igx_0 \left[\bar{a}_1 (\bar{b} + \bar{b}^*) + \bar{a}_1 (\delta b(t) + \delta b^*(t)) + \delta a_1(t) (\bar{b} + \bar{b}^*) \right], \end{aligned} \quad (3.57)$$

$$\frac{d}{dt} (\bar{a}_2 + \delta a_2(t)) = (i\Delta - \gamma_2) (\bar{a}_2 + \delta a_2(t)) - i\kappa (\bar{a}_1 + \delta a_1(t)), \quad (3.58)$$

$$\frac{d}{dt} (\bar{b} + \delta b(t)) = (-i\omega_m - \gamma_m) (\bar{b} + \delta b(t)) + igx_0 (\bar{a}_1^* \bar{a}_1 + \delta a_1^*(t) \bar{a}_1 + \bar{a}_1^* \delta a_1(t)), \quad (3.59)$$

where we have neglected the noise forces and dropped the terms of higher than first order in the perturbations. Using the relation

$$\dot{\bar{a}}_1 = \dot{\bar{a}}_2 = \dot{\bar{b}} = 0, \quad (3.60)$$

the zero-order contribution of eqs. (3.57) to (3.59) reads

$$0 = (i\Delta - \gamma_1) \bar{a}_1 - i\kappa \bar{a}_2 + igx_0 \bar{a}_1 (\bar{b} + \bar{b}^*) + \Omega, \quad (3.61)$$

$$0 = (i\Delta - \gamma_2) \bar{a}_2 - i\kappa \bar{a}_1, \quad (3.62)$$

$$0 = (-i\omega_m - \gamma_m) \bar{b} + igx_0 \bar{a}_1^* \bar{a}_1. \quad (3.63)$$

Equations (3.61) to (3.63) represent a closed set of nonlinear equations for the steady state fields and can be easily solved numerically. The first order equations are then given by

$$\delta \dot{a}_1(t) = (i\Delta - \gamma_1) \delta a_1(t) - i\kappa \delta a_2(t) + \alpha (\delta b(t) + \delta b^*(t)) + \beta \delta a_1(t), \quad (3.64)$$

$$\delta \dot{a}_2(t) = (i\Delta - \gamma_2) \delta a_2(t) - i\kappa \delta a_1(t), \quad (3.65)$$

$$\delta \dot{b}(t) = (-i\omega_m - \gamma_m) \delta b(t) + \alpha^* \delta a_1(t) + \alpha \delta a_1^*(t), \quad (3.66)$$

where we have introduced the abbreviations $\alpha = igx_0 \bar{a}_1$ and $\beta = igx_0 (\bar{b} + \bar{b}^*)$. The values for the steady-state quantities \bar{a}_1 and \bar{b} are directly taken from the solution of eqs. (3.61) to (3.63).

⁷ Note that this *ansatz* is valid only below threshold as it is demonstrated in section 4.1.1.

The next step is to define the solution vector

$$\mathbf{u}(t) := \left(\delta a_1(t) \quad \delta a_1^*(t) \quad \delta a_2(t) \quad \delta a_2^*(t) \quad \delta b(t) \quad \delta b^*(t) \right)^T, \quad (3.67)$$

which satisfies eq. (3.53) with the matrix

$$A = \begin{pmatrix} i\Delta - \gamma_1 + \beta & 0 & -i\kappa & 0 & \alpha & \alpha \\ 0 & -i\Delta - \gamma_1 - \beta & 0 & i\kappa & \alpha^* & \alpha^* \\ -i\kappa & 0 & i\Delta - \gamma_2 & 0 & 0 & 0 \\ 0 & i\kappa & 0 & -i\Delta - \gamma_2 & 0 & 0 \\ -\alpha^* & \alpha & 0 & 0 & -i\omega_m - \gamma_m & 0 \\ \alpha^* & -\alpha & 0 & 0 & 0 & i\omega_m - \gamma_m \end{pmatrix}. \quad (3.68)$$

By calculating the eigenvalues of the matrix A , it can be decided for any given input parameter set whether the system is below or above threshold. The exact value for the threshold pump power can be found by systematically varying the input power and simultaneously evaluating the eigenvalues of the matrix A .

3.3 Calculation of the signal linewidth

Our main goal is to calculate the linewidth of the phonon laser above threshold. The extraction of the linewidth of a noisy signal can be performed either in the frequency domain or in the time domain [41]. The determination of the linewidth in the frequency domain requires the analysis of the phonon mode spectrum. According to the *Wiener-Khinchin theorem*, the power spectrum of a signal $x(t)$ is given by the Fourier transform of its autocorrelation function,

$$S(\omega) = \frac{1}{\sqrt{2\pi}} \int_{-\infty}^{\infty} R_{xx}(t) e^{i\omega t} dt, \quad (3.69)$$

where the autocorrelation function is defined as

$$R_{xx}(t) := \langle x(\tau) x^*(\tau - t) \rangle = \lim_{T \rightarrow \infty} \frac{1}{2T} \int_{-T}^T x(\tau) x^*(\tau - t) d\tau. \quad (3.70)$$

Typically, a laser spectrum contains a peak centered around the laser frequency, and the linewidth is defined as the full width at half maximum (FWHM) of this peak. However, due to the narrow linewidth of a laser, it is necessary to calculate the autocorrelation function and its Fourier transform for a large number of sample points in order to properly resolve the resonant peak. Consequently, this requires considerable computational effort. A numerically more efficient method to extract the linewidth from the signal is given by the time domain analysis. As a result of the noise in the signal, both the amplitude and the phase of the field are subject to statistical fluctuations, where the linewidth is mainly

governed by the behavior of the phase. The phase φ can be expressed as the sum of a deterministic part caused by the laser frequency ω and a fluctuating term $\delta\varphi$ due to the presence of the noise,

$$\varphi(t) = \omega t + \delta\varphi(t). \quad (3.71)$$

One finds under certain approximations (for details see e.g. chapter 12 in [27]) that the square of the phase fluctuations diffuses linearly in time, i.e.

$$\langle (\delta\varphi(t) - \delta\varphi(0))^2 \rangle = \Delta\omega \cdot t, \quad (3.72)$$

where the rate of diffusion is given by the linewidth $\Delta\omega$. This is the main idea of the time domain analysis. To summarize, the laser linewidth can be calculated in the following way:

- (i) The system equations are numerically solved for a large number of different noise realizations. Depending on the initial conditions for the time integration, the system shows some transient behavior until a steady state is reached. The transient part of the solution has to be omitted to obtain correct results.
- (ii) For a certain time interval in the steady state, the phase is evaluated at each time step of the different solutions from (i). In this process, the deterministic part of the phase is removed since we are only interested in the phase fluctuations $\delta\varphi$.
- (iii) The average phase diffusion for each time t_i is calculated according to

$$\langle (\delta\varphi(t_i) - \delta\varphi(0))^2 \rangle = \frac{1}{N} \sum_{\mu=1}^N (\delta\varphi_{\mu}(t_i) - \delta\varphi_{\mu}(0))^2, \quad (3.73)$$

where N is the number of different solutions generated in (i). The steps (ii) and (iii) can be combined with (i), which has the advantage that the solutions are not required to be stored.

- (iv) The data from (iii) is fitted with the function $f(t) = c \cdot t$, in which the fit parameter c corresponds to the linewidth of the signal.

The decisive factor for the accuracy of this method is mainly the number of resulting solutions for different noise realizations.

4 Results and Discussion

The theoretical results presented in this chapter have been generated by numerically solving the system eqs. (2.30) to (2.32) according to the procedures outlined in chapter 3. The experimental data as well as the figures with the experimental results shown here have been produced by the *Micro/Nano Photonics Lab* at *Washington University in St. Louis*⁸. Since there are already experimental results available, the intention of this thesis is to compare theory and experiment. Therefore, most of the calculations presented in this chapter have been performed with similar parameter values as those used in the experiment. In the following, this parameter set will be referred to as *experimental parameter set*. Furthermore, we additionally define a *modified parameter set* in order to compare the results for different parameter values. The parameter values of the experimental and modified parameters sets are shown in table 4.1.

Table 4.1: Phonon laser system parameters used in the calculations.

Parameter	Experimental parameter set	Modified parameter set
ω_c	$2\pi \cdot 2 \cdot 10^{14}$ Hz	$2\pi \cdot 2 \cdot 10^{14}$ Hz
ω_m	$2\pi \cdot 17.4$ MHz	$2\pi \cdot 2.77$ MHz
γ_1	$2\pi \cdot 3.2$ MHz	$2\pi \cdot 160$ kHz
γ_2	$2\pi \cdot 13.6$ MHz	$2\pi \cdot 480$ kHz
γ_m	$2\pi \cdot 40$ kHz	$2\pi \cdot 40$ kHz
κ	$2\pi \cdot 12.6$ MHz	$2\pi \cdot 1.39$ MHz
gx_0	$2\pi \cdot 1.6$ kHz	$2\pi \cdot 40$ Hz

With the parameters from table 4.1, we can calculate the value of γ_{tip} where the EP occurs. This value is given for the experimental parameter set as $\gamma_{\text{tip}}^{\text{EP}} \approx 2\pi \cdot 14.8$ MHz and for the modified parameter set as $\gamma_{\text{tip}}^{\text{EP}} \approx 2\pi \cdot 2.46$ MHz. In the following, the situation with $\gamma_{\text{tip}} < \gamma_{\text{tip}}^{\text{EP}}$ will be referred to as the regime *before* the EP and analogously for $\gamma_{\text{tip}} > \gamma_{\text{tip}}^{\text{EP}}$ the regime *after* the EP.

It should be noted that the value for the optomechanical coupling strength gx_0 from the actual experiment was reported to be about $gx_0 \approx 2\pi \cdot 8.4$ MHz. In what we call the experimental parameter set, however, we have employed a much smaller value. The value of gx_0 in our calculations had to be reduced because the noise strength

⁸ Provided by Şahin Özdemir, private communication, 2015.

becomes unrealistically high and exceeds the signal amplitudes for high values of gx_0 (see [section 4.1.1](#) and [fig. 4.4](#)). However, this is justified as it turns out that the results remain qualitatively unchanged when gx_0 is varied, which was verified in a range of several orders of magnitude.

As shown in [sections 4.1](#) and [4.2.2](#) below, the results for the phonon laser behavior in the vicinity of an EP strongly depend on the driving frequency ω_d . One possibility to operate the phonon laser is to pump one of the optical supermodes non-resonantly. This means that the driving frequency is detuned from the supermode frequency by the value of the mechanical resonance frequency. Unless explicitly stated otherwise, we used the driving frequency $\omega_d = \omega_m + \omega_+$ for our calculations because this is exactly the procedure that was followed in the experiment. Ideally, in this case, the frequency splitting between the two optical supermodes should also be equal to the resonance frequency of the mechanical mode (for $\gamma_{\text{tip}} = 0$) because phonons can then be additionally amplified by stimulated emission due to transitions between the two photonic supermode levels producing a phonon (cf. [section 2.1.1](#)). We note in this context that this resonance is not exactly satisfied by the experimental parameter set. Using [eq. \(2.55\)](#) and $\omega_{\pm} = \text{Re}(\lambda_{\pm})$, the supermode frequency splitting is found to be

$$\omega_{\text{split}} = \omega_+ - \omega_- = \sqrt{4\kappa^2 - (\gamma_2 - \gamma_1)^2} \approx 2\pi \cdot 23 \text{ MHz} \quad (4.1)$$

for the experimental parameter set, which is about one third larger than the value for the mechanical resonance frequency ω_m . In contrast, the modified parameter set has been chosen such that $\omega_{\text{split}} \approx \omega_m$ holds.

In the first part of this chapter ([section 4.1](#)), we study some basic properties of the phonon laser. As a first test of the theory, we present the theoretical results which are calculated by omitting the noise terms in [eqs. \(2.30\)](#) to [\(2.32\)](#), as for example the optomechanical amplification or the phonon laser threshold dependence. These results are then compared to the experimental data. In the second part ([section 4.2](#)), all noise terms are taken into account in order to calculate the linewidth of the phonon laser. The influence of several system and operation parameters is examined and the outcome is compared to the experimental results.

4.1 Phonon laser characteristics

4.1.1 Time-dependent solution of the system equations

To study the dynamical regimes in our phonon laser, we numerically solve the system equations. Typical solutions without noise for the experimental and modified parameter sets (with $\gamma_{\text{tip}} = 0$) are shown in [figs. 4.1](#) and [4.2](#). In analogy to the case of a conventional photon laser, one can distinguish between two qualitatively different dynamical regimes: the regime below threshold and the regime above threshold. For sufficiently small values of the input pump power P_{in} , the system is not lasing. In this case, the solutions reach a

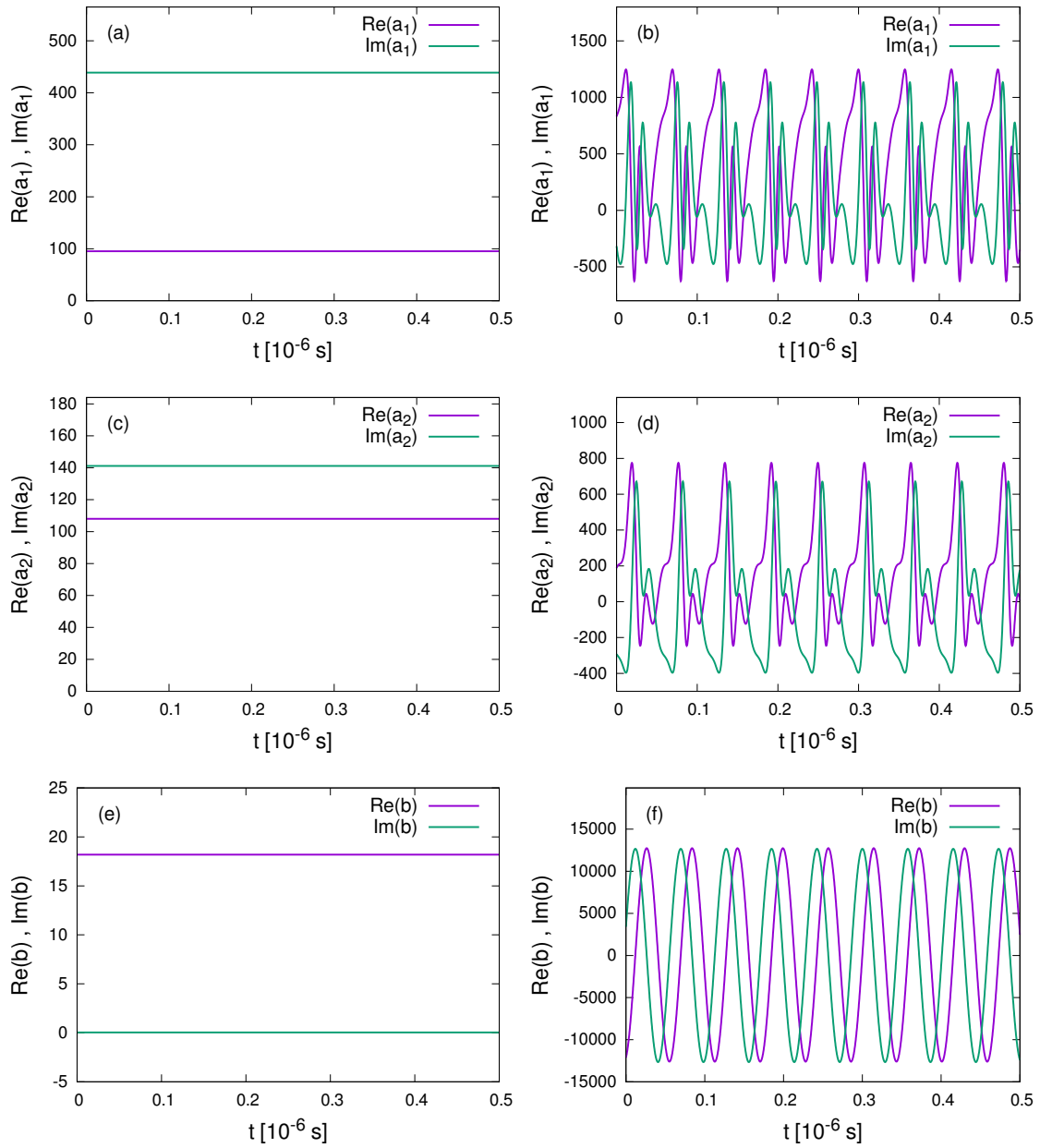


Figure 4.1: Time-dependent solution of the phonon laser system at a steady state for the experimental parameter set. The left column (a,c,e) shows the fields a_1 , a_2 , and b below threshold ($P_{in} = 0.9 \cdot P_{thr}$), the right column (b,d,f) shows the fields above threshold ($P_{in} = 1.1 \cdot P_{thr}$).

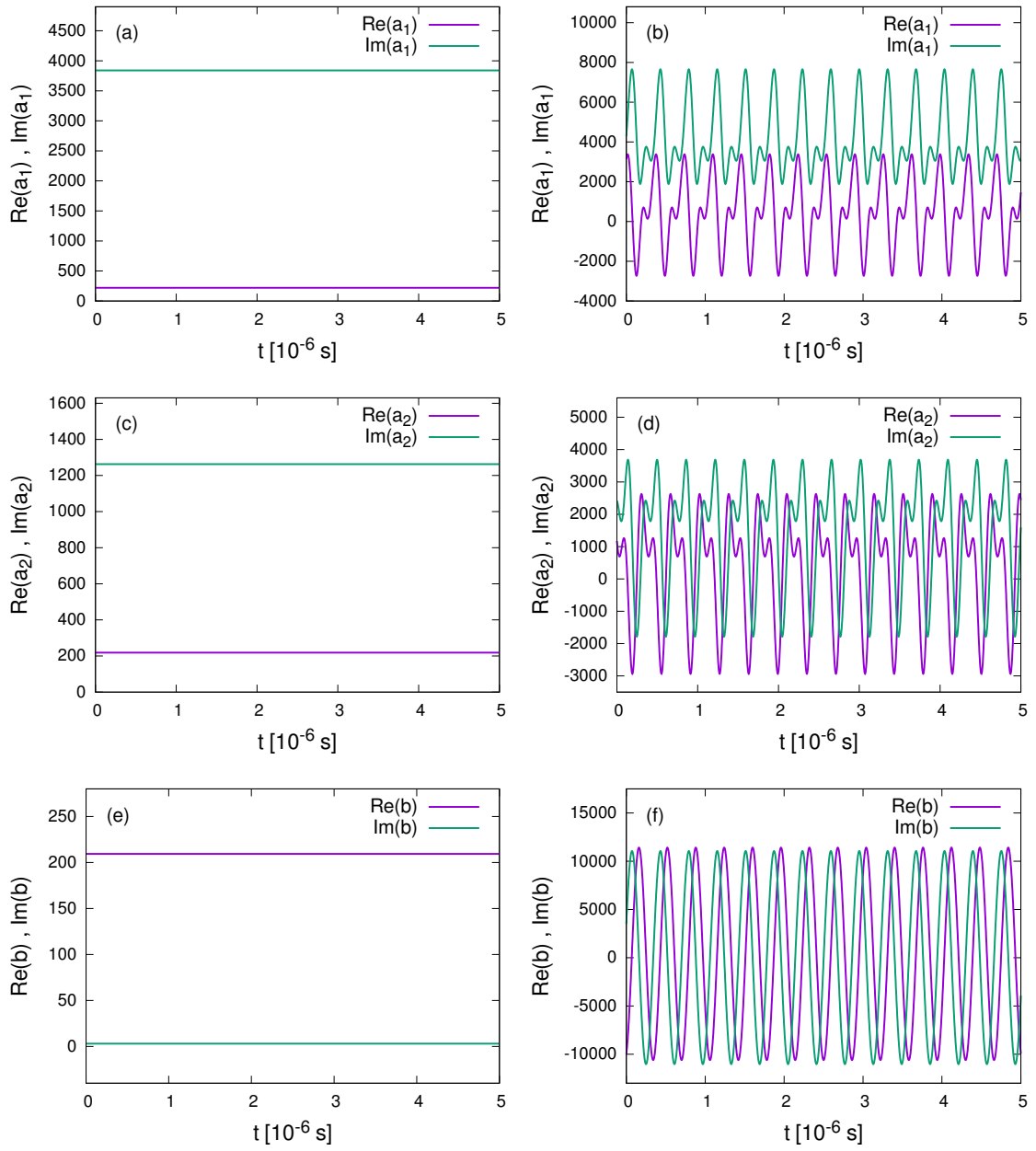


Figure 4.2: Time-dependent solution of the phonon laser system at a steady state for the modified parameter set. The left column (a,c,e) shows the fields a_1 , a_2 , and b below threshold ($P_{\text{in}} = 0.9 \cdot P_{\text{thr}}$), the right column (b,d,f) shows the fields above threshold ($P_{\text{in}} = 1.1 \cdot P_{\text{thr}}$).

constant steady state value⁹. Above a critical value P_{thr} , however, phonon lasing occurs and the solutions show an oscillatory behavior. Below threshold, the solutions for the optical modes are constant only in the rotating frame but oscillate with frequency ω_d in the lab frame. The values of the optical solutions in the rotating frame merely determine the relative phase between the two optical modes. The mechanical mode, however, is not given in a rotating frame and is thus constant in the lab frame. This can be understood as a constant displacement of the resonator which contains the mechanical mode due to the radiation pressure of the optical field in the cavity. The steady-state values for the solutions below threshold can also be obtained by solving eqs. (3.61) to (3.63). Above threshold, on the other hand, both optical and mechanical modes are oscillating. The mechanical mode oscillates with the laser frequency ω which is approximately equal to the resonance frequency ω_m . Additionally, there is still a constant contribution to the mechanical field as a result of the radiation pressure forces. Therefore, the mechanical field can be approximated by the sum of an oscillating part with amplitude B and a constant contribution b_0 ,

$$b(t) \approx B e^{-i\omega t} + b_0, \quad (4.2)$$

which is used to calculate the phase diffusion in section 4.2.2. However, the optical modes cannot be approximated by a simple form similar to eq. (4.2) because they show a more complex behavior above threshold due to the non-linear character of the system equations.

Figures 4.1 and 4.2 show the solutions of the system equations in a steady state. In order to solve the equations numerically, one has to define initial values of the fields for the first time step. In our calculations, we choose the fields initially to be equal to zero. Consequently, in the time-dependent solution, the system needs a certain number of time steps to reach a stationary value. This transient behavior for the phonon mode is depicted in fig. 4.3. The transient region in the time-dependent signal has to be excluded for further analysis, especially for linewidth calculations.

Hitherto, we have only considered the solutions of the system equations without noise. The addition of the respective noise terms causes statistical fluctuations of the signal amplitude and phase whose magnitudes depend on the signal-to-noise ratio. According to eqs. (3.33) to (3.35), the noise strength depends only on the ambient temperature as well as on the optical and mechanical dissipation rates γ_1 , γ_2 , and γ_m . The signal amplitudes, however, depend on other parameters as well. For example, the signal amplitudes (for $P_{\text{in}} = 1.1P_{\text{thr}}$) decrease if the optomechanical coupling gx_0 is increased while the noise strength remains constant (see fig. 4.4). As long as the value of gx_0 is small enough, the signal is only marginally disturbed by the noise. The larger the value of gx_0 is, the stronger the effect of the noise on the signal is observable. For very high values of the optomechanical coupling, the noise strength exceeds the signal amplitude, which leads to unreasonable results due to enormous amplitude and phase fluctuations. Consequently, the system parameters have to be chosen such that the noise strength lies well below the signal amplitude in order to enable a proper numerical analysis.

⁹ Note that we consider the solutions for the optical modes in a rotating frame. In order to obtain the solutions in the lab frame, the optical modes have to be multiplied with the factor $e^{-i\omega_d t}$.

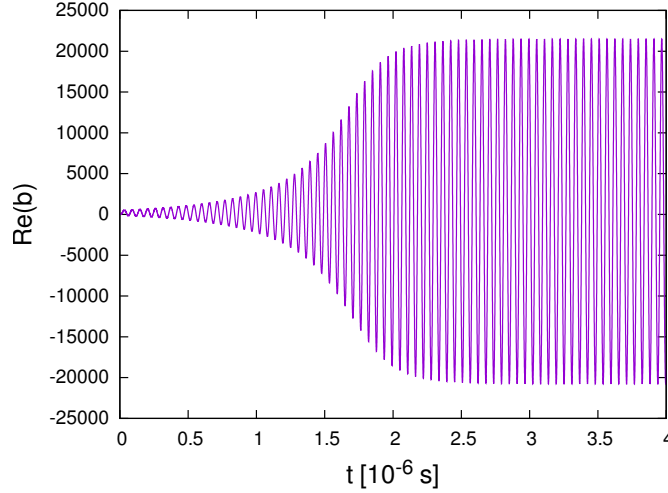


Figure 4.3: Transient behavior of the numerical solution for the phonon mode. Initially, the solution $b(t_0)$ is set equal to zero. After a certain time interval, the amplitude reaches a stationary value.

4.1.2 Phonon laser threshold

A characteristic feature of a laser is the existence of a laser threshold, i.e. a critical value for the pump power at which the laser emission sets in. Besides a significant linewidth narrowing, the laser threshold is characterized by a substantial increase of the laser intensity. Figure 4.5 shows the dependence of the phonon laser intensity as a function of the input pump power P_{in} for the regimes before and after the EP. As can be seen, in both cases the intensity remains small as long as $P_{\text{in}} < P_{\text{thr}}$. Above threshold, the intensity grows rapidly with increasing pump power. However, the curves look qualitatively different in the regimes before and after the EP. Before the EP ($\gamma_{\text{tip}} = 0$), the intensity grows linearly with the pump power, except for a narrow pump interval close to the threshold, where a non-linear growth is observed. After the EP, however, we find an asymptotic square root dependence of the intensity on the pump power, $I \propto \sqrt{P_{\text{in}} - P_{\text{thr}}}$. This might be a result of the two different operating regimes of the phonon laser. Before the EP, the two supermode frequencies are split and phonons can also be amplified by means of stimulated emission due to photon transitions between the two supermode levels. This is not possible in the regime after the EP where the supermode frequencies are identical. In fact, the only possibility of coherent amplification is stimulated *Raman* scattering. Experimental results for the phonon laser output power as a function of the pump power are shown in fig. 4.6.

In the remaining part of this section, we want to concentrate on the behavior of the threshold pump power in the vicinity of the EP. For this purpose, we calculate P_{thr} with the method described in section 3.2 while varying the value of γ_{tip} . It turned out that the results for the experimental parameter set with $\omega_{\text{d}} = \omega_{\text{m}} + \omega_{+}$ agree quite well with the experimental data (see fig. 4.7). In the regime before the EP, the threshold pump power has a maximum after which it drops rapidly until $\gamma_{\text{tip}} = \gamma_{\text{tip}}^{\text{EP}}$ where we

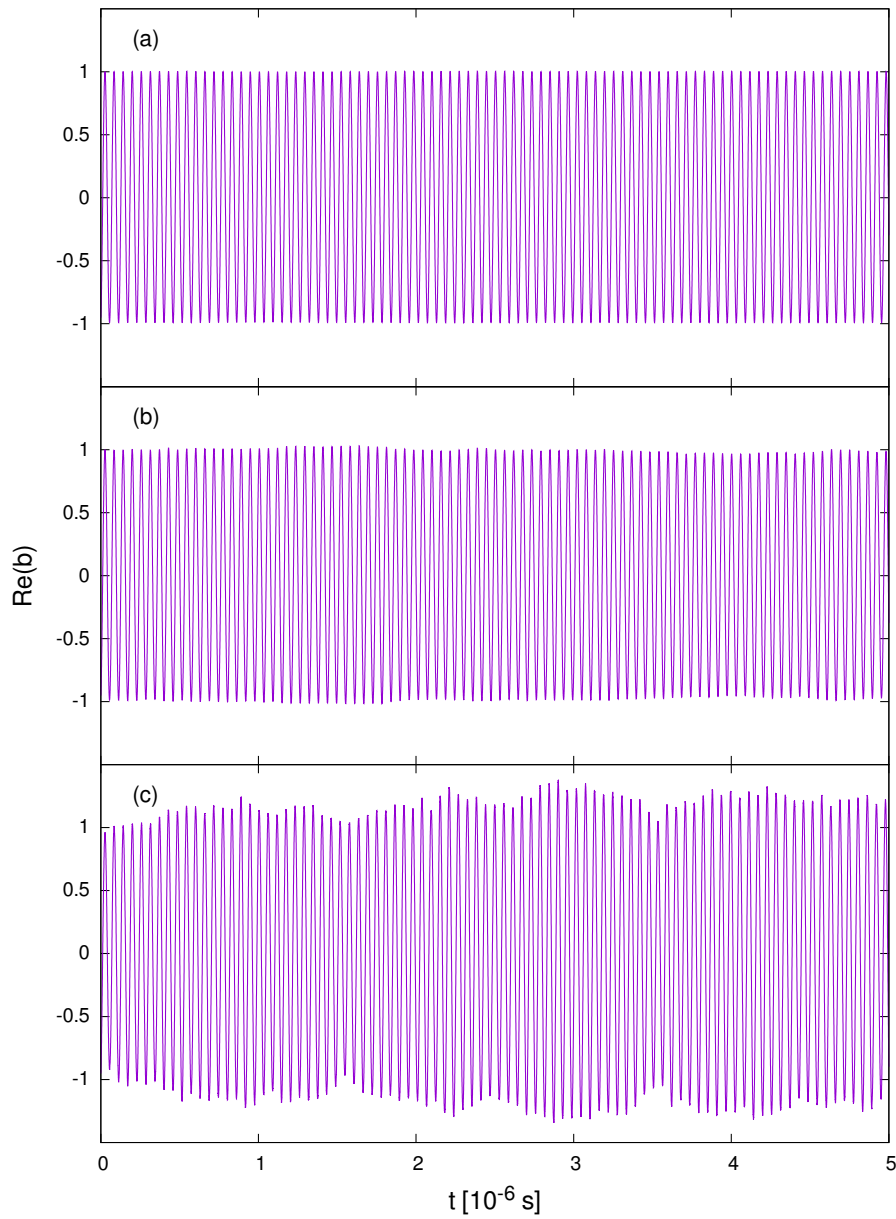


Figure 4.4: Influence of the noise on the signal for the experimental parameter set with different optomechanical coupling strengths: (a) $gx_0 = 2\pi \cdot 160$ Hz, (b) $gx_0 = 2\pi \cdot 1.6$ kHz, and (c) $gx_0 = 2\pi \cdot 16$ kHz. For each case, the pump power was chosen to be $P_{\text{in}} = 1.1 \cdot P_{\text{thr}}$ and the field amplitude is always normalized to the steady state value without noise.

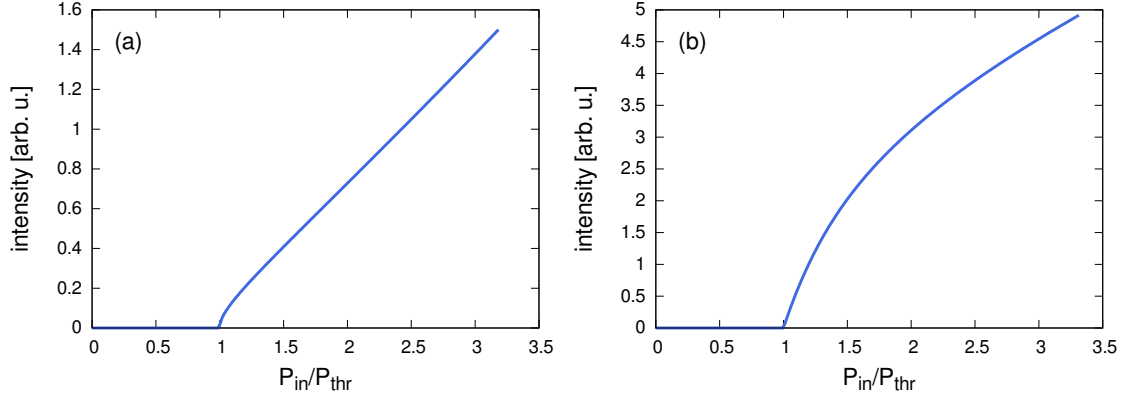


Figure 4.5: Phonon laser intensity as a function of the input pump power for the modified parameter set with $\gamma_{tip} = 0$ (a) and $\gamma_{tip} = 2\pi \cdot 3.2 \text{ MHz} > \gamma_{tip}^{EP} \approx 2\pi \cdot 2.46 \text{ MHz}$ (b).

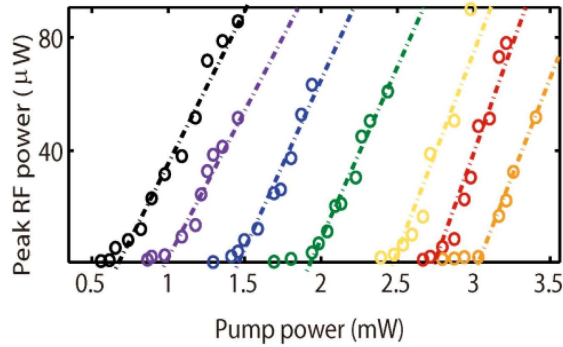


Figure 4.6: Experimental results for the phonon laser threshold for different values of γ_{tip} . Figure courtesy of Şahin Özdemir (*Washington University in St. Louis*).

observe a kink in the threshold curve. After the EP, the threshold pump power decreases slowly with increasing γ_{tip} . It turns out that the results strongly depend on the driving frequency ω_d , which is shown in fig. 4.8. For both the experimental and the modified parameter set, the threshold in the regime before the EP is much lower for $\omega_d = \omega_m + \omega_-$ compared to the case for $\omega_d = \omega_m + \omega_+$. If the driving frequency is chosen to be constant, $\omega_d = \omega_m + \omega_c$, the phonon laser threshold is a monotonously decreasing function of γ_{tip} (in the investigated parameter range). Besides, there is no kink in the curve for this driving frequency. The occurrence of the kink in the curves for the previously considered driving frequencies is not the result of a special feature of the EP but arises because of the behavior of the input parameter $\omega_d = \omega_m + \omega_{\pm}$. The reason is that the curves for the supermode frequencies already show a kink at the EP (cf. eq. (2.55) and fig. 2.4) which is directly reflected in the shapes of the calculation results.

Finally, it should be mentioned that the phonon laser threshold results (figs. 4.5 and 4.8) remain qualitatively unchanged if the value of g_{x_0} is varied. There is only a constant scaling factor for the threshold pump power $P_{thr} \propto 1/(g_{x_0})^2$.

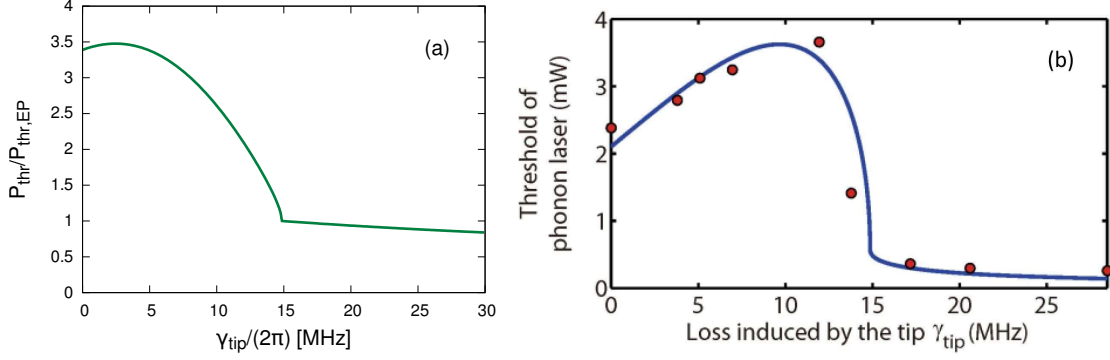


Figure 4.7: Comparison between the theoretical (a) and experimental (b) results for the threshold pump power of the phonon laser system as a function of γ_{tip} . The driving frequency was chosen to be $\omega_{\text{d}} = \omega_{\text{m}} + \omega_{+}$. Right figure courtesy of Şahin Özdemir (*Washington University in St. Louis*).

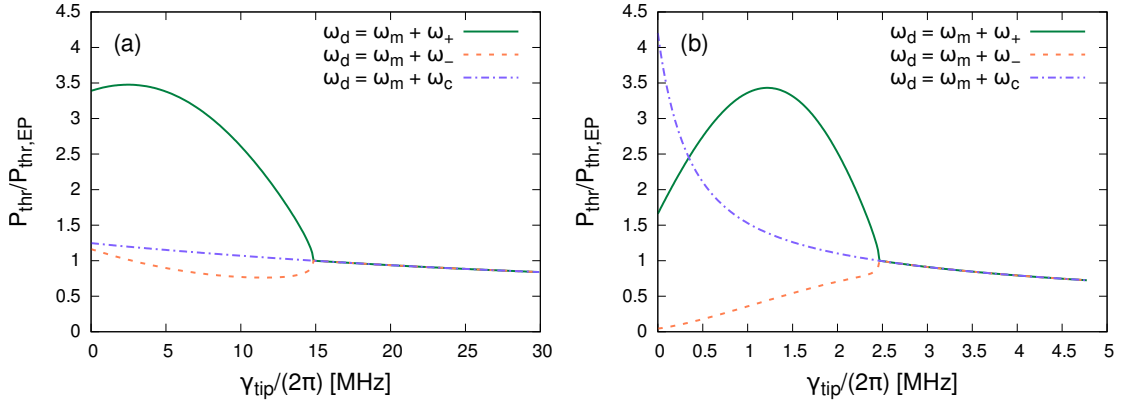


Figure 4.8: Threshold pump power of the phonon laser system as a function of γ_{tip} for the experimental parameter set (a) and the modified parameter set (b). The curve is shown for three different driving frequencies ω_{d} .

4.1.3 Optomechanical amplification

As a result of the optomechanical interaction in the system, phonons are coherently amplified if the input power is high enough, i.e. if the system is pumped above threshold. The magnitude of amplification, i.e. the achievable phonon intensity, strongly depends on the system parameters, in particular on the additional loss induced by the tip and on the driving frequency. Depending on the choice of ω_{d} , we observe a large variation of the phonon laser intensity as a function of γ_{tip} in the vicinity of the EP (see fig. 4.9). For the experimental parameter set, the curves for the phonon laser intensity look similar to the curves for the phonon laser threshold as a function of γ_{tip} (fig. 4.8). With $\omega_{\text{d}} = \omega_{\text{m}} + \omega_{+}$, the intensity first increases slightly, then drops rapidly until $\gamma_{\text{tip}} = \gamma_{\text{tip}}^{\text{EP}}$, and decreases slowly for $\gamma_{\text{tip}} > \gamma_{\text{tip}}^{\text{EP}}$. In contrast, if $\omega_{\text{d}} = \omega_{\text{m}} + \omega_{-}$, the intensity increases monotonously for $\gamma_{\text{tip}} < \gamma_{\text{tip}}^{\text{EP}}$. Moreover, the resulting intensity before the EP is much

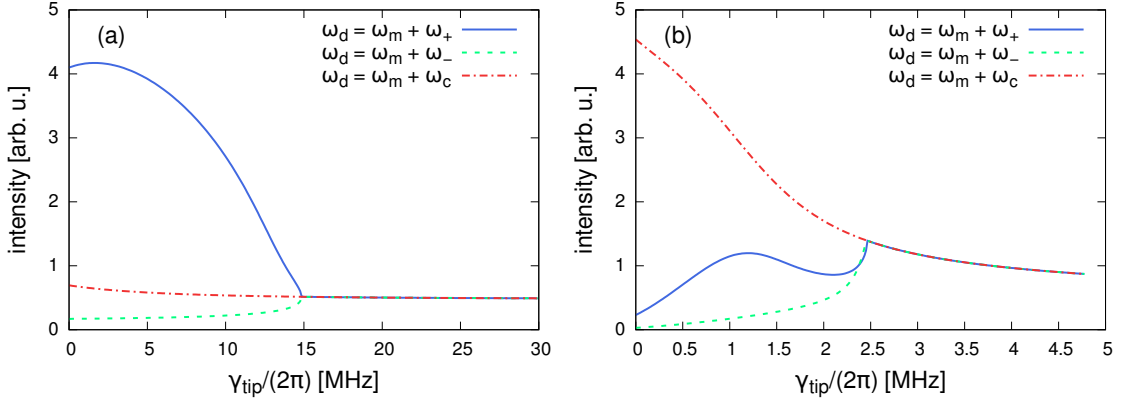


Figure 4.9: Intensity of the phonon field as a function of γ_{tip} with input power $P_{\text{in}} = 1.2 \cdot P_{\text{thr}}$ for the experimental parameter set (a) and the modified parameter set (b). The curve is shown for three different driving frequencies ω_d .

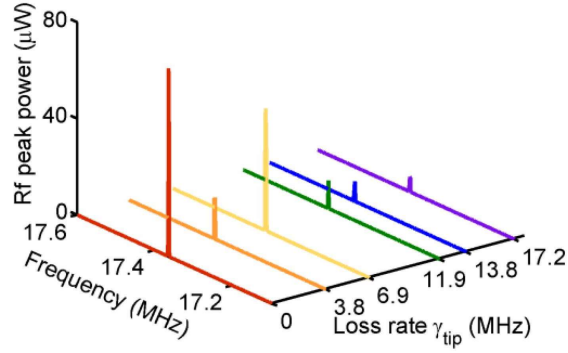


Figure 4.10: Experimental results for the phonon laser intensity for different values of γ_{tip} . In this measurement, the pump power was always chosen to be 20 % above threshold, i.e. $P_{\text{in}} = 1.2 \cdot P_{\text{thr}}$. Figure courtesy of Şahin Özdemir (*Washington University in St. Louis*).

smaller as compared to the case with $\omega_d = \omega_m + \omega_+$. However, if $\omega_d = \omega_m + \omega_c$, the intensity decreases monotonously for all values of γ_{tip} in the investigated range and the intensity before the EP is also much smaller than for $\omega_d = \omega_m + \omega_+$ but larger than for $\omega_d = \omega_m + \omega_-$. For the modified parameter set, the highest phonon intensity is attained with $\omega_d = \omega_m + \omega_c$. The qualitative behavior of the intensity curves for $\omega_d = \omega_m + \omega_c$ and $\omega_d = \omega_m + \omega_-$ is there also comparable to the corresponding threshold curves (fig. 4.8). The case with $\omega_d = \omega_m + \omega_+$, however, gives rise to a qualitative different behavior. There, the intensity curve has two local maxima, one of which is located exactly at the EP. A similar behavior with two maxima was also observed in the experiment as shown in fig. 4.10. However, the second maximum in the experimental results is not located at the EP but occurs in the region before the EP. A possible explanation for this discrepancy could be the accidental change of the inter-resonator coupling strength κ . If the distance between the two optical resonators is changed (e.g. due to environmental vibrations), the value of κ is modified, which also affects the value of γ_{tip} where the EP

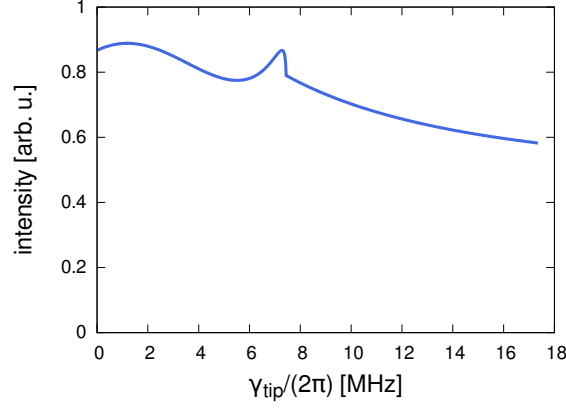


Figure 4.11: Intensity of the phonon field as a function of γ_{tip} for the driving frequency $\omega_{\text{d}} = \omega_{\text{m}} + \omega_{+}$ and $P_{\text{in}} = 1.2 \cdot P_{\text{thr}}$ where the experimental parameter set with an adjusted value of $\kappa = 2\pi \cdot 8.5$ MHz was used.

occurs. Indeed, one can generate a result which is similar to the intensity curve for the modified parameter set with $\omega_{\text{d}} = \omega_{\text{m}} + \omega_{+}$ if the experimental parameter set with an adjusted value of κ is used. For comparison to the experimental data, this result is shown in [fig. 4.11](#).

4.2 Numerical linewidth calculations

4.2.1 Linewidth calculations for a conventional photon laser

In the theory of a conventional photon laser, one can derive a closed equation for the electromagnetic field alone by adiabatically eliminating the atomic polarization and population variables [27]. This equation reads for the laser field α

$$\dot{\alpha} = -\frac{\mathcal{C}}{2} + \frac{\mathcal{A}\alpha}{2\left(1 + \frac{\mathcal{B}}{\mathcal{A}}I\right)} + \mathcal{F}_{\alpha}, \quad (4.3)$$

where $I = |\alpha|^2$, \mathcal{A} and \mathcal{B} are the gain and saturation coefficients, \mathcal{C} is the cavity decay rate, and \mathcal{F}_{α} is the corresponding Langevin noise force whose diffusion coefficients are given by

$$D_{\alpha\alpha} = -\frac{\mathcal{B}\alpha^2}{4\left(1 + \frac{\mathcal{B}}{\mathcal{A}}I\right)^2} \left(3 + \frac{\mathcal{B}}{\mathcal{A}}I\right), \quad (4.4)$$

$$D_{\alpha^*\alpha} = \frac{\mathcal{A}}{\left(1 + \frac{\mathcal{B}}{\mathcal{A}}I\right)^2} \left[1 + \frac{\mathcal{B}}{4\mathcal{A}}I \left(3 + \frac{\mathcal{B}}{\mathcal{A}}I\right)\right]. \quad (4.5)$$

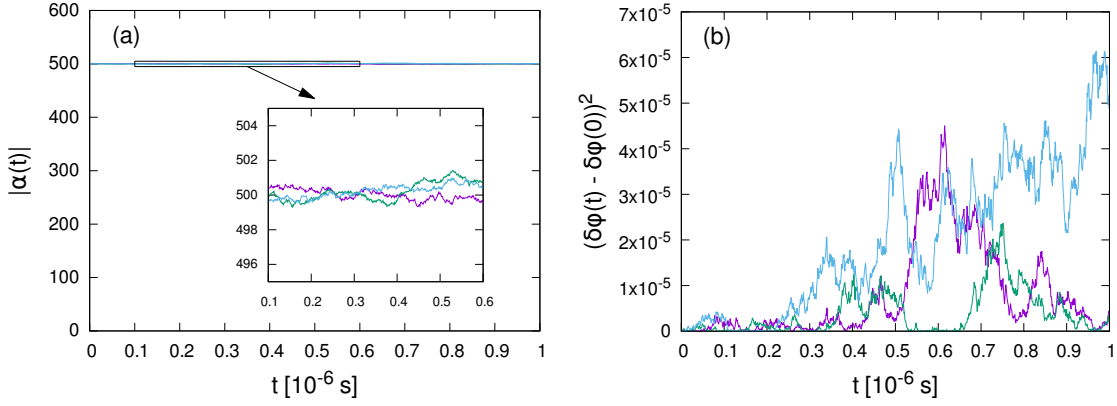


Figure 4.12: Typical stationary solutions of the laser equation eq. (4.3). The Langevin noise force causes both amplitude (a) and phase fluctuations (b).

Equations (4.3) to (4.5) can be used to derive an analytic expression for the phase diffusion of the laser field which is given by

$$\langle (\delta\varphi(t) - \delta\varphi(0))^2 \rangle = \frac{\mathcal{A} + \mathcal{C}}{4 \langle n \rangle} \cdot t = \Delta\omega \cdot t, \quad (4.6)$$

where $\Delta\omega$ is the linewidth of the laser and

$$\langle n \rangle = I_0 = \frac{\mathcal{A}}{\mathcal{C}} \left(\frac{\mathcal{A} - \mathcal{C}}{\mathcal{B}} \right) \quad (4.7)$$

is the mean photon number. The derivation of an equivalent analytical formula for the linewidth of our phonon laser is not possible in this way because of the substantially more complicated structure of the phonon laser equations eqs. (2.30) to (2.32). Therefore, we have to determine the phonon laser linewidth numerically with the procedure described in section 3.3. As a first test of our method, we want to numerically calculate the linewidth of a conventional photon laser such that we can compare the results to the predictions of the analytically derived formula for the linewidth. For that purpose, we have to numerically solve eq. (4.3) and average the results for many different noise realizations in order to calculate the phase diffusion and hence the laser linewidth. The noise has to be implemented such that the constraints for the diffusion coefficients eqs. (4.4) and (4.5) are satisfied (cf. the procedure demonstrated for the phonon laser in section 3.1). Since eq. (4.3) is given in a frame rotating with the laser frequency ω , the steady state solution for the electromagnetic field α yields a constant value. Due to the action of the noise force \mathcal{F}_α , however, the field is subject to both amplitude and phase fluctuations. This is demonstrated for three different noise realizations in fig. 4.12. If the square of the phase is averaged over many different noise realizations, the linear diffusion in time can be observed as expected (see fig. 4.13). Note that the accuracy of the results in fig. 4.13 depends on the number of different noise realizations. If the average is performed over a relatively small number of solutions, e.g. for 10^2 trajectories, there are

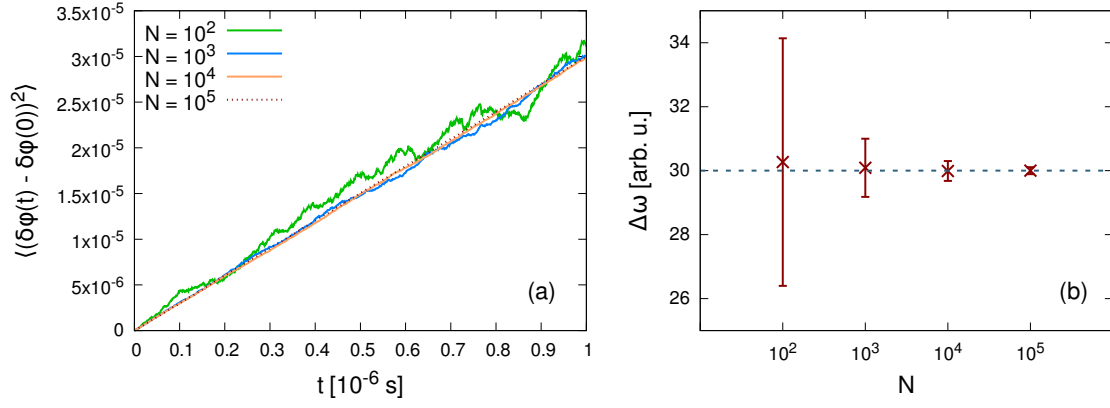


Figure 4.13: Due to the presence of the noise, the square of the phase φ diffuses linearly in time (a). The average slope of the phase diffusion corresponds to the laser linewidth. The crosses in (b) mark the average linewidth values of 10 simulation runs (each run averaged over N trajectories), the error bars represent the corresponding standard error, and the dashed line indicates the analytically calculated linewidth result. The accuracy of the method depends on the total number of different trajectories N .

still significant phase fluctuations observable. For 10^5 trajectories, however, the phase diffusion curve becomes already very smooth. The slope of the linear approximation to $\langle (\delta\varphi(t) - \delta\varphi(0))^2 \rangle$ corresponds to the linewidth of the laser. The simulation results agree very well with the analytic formula eq. (4.6) (see fig. 4.13). This has been verified for a wide range of the parameters \mathcal{A} , \mathcal{B} , and \mathcal{C} . Thus, the validity of the linewidth calculation method from section 3.3 has been proved.

4.2.2 Phonon laser linewidth calculations

In section 4.2.1, we have calculated the linewidth of a photon laser with the phase diffusion method from section 3.3. Apart from amplitude and phase fluctuations, the laser field $a(t)$ was there given by a constant steady state value (in the rotating frame). The field of our phonon laser $b(t)$, however, is not given in a rotating frame and therefore represents an oscillating quantity which can be approximated in the steady state by eq. (4.2). In order to use the same method as before, the oscillating factor as well as the constant contribution of the field have to be excluded. This is done by calculating the phase diffusion of the modified field

$$b'(t) = (b(t) - b_0) e^{i\omega t}. \quad (4.8)$$

Typical results of the phonon laser phase diffusion for the experimental parameter set with two different values of γ_{tip} are shown in figs. 4.14 and 4.15. There, the average square of the phase is not a pure linear function of time but also shows periodic oscillations which occur because of higher frequency components in the phonon field that are not considered by eq. (4.8). The relative magnitude of these oscillations compared to the overall phase diffusion depends on the input pump power and grows with increasing P_{in} .

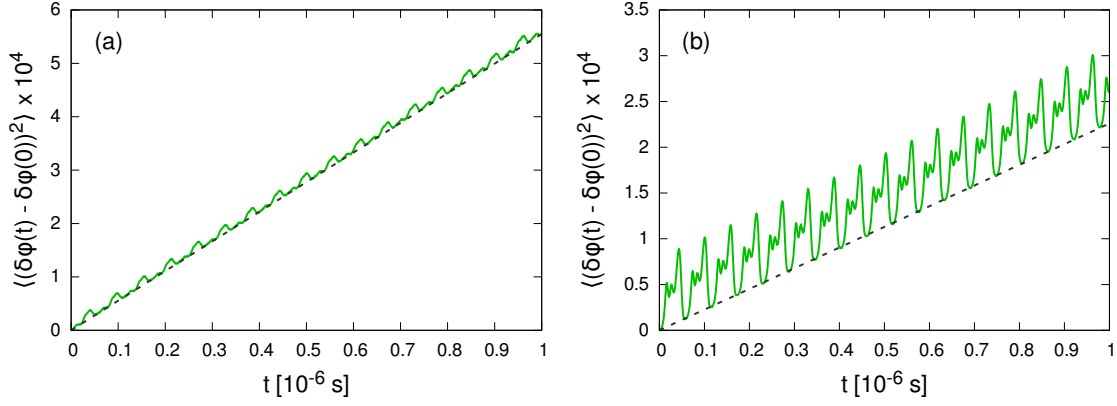


Figure 4.14: Phonon laser phase diffusion for the experimental parameter set with $\gamma_{\text{tip}} = 0$ for different pump powers $P_{\text{in}} = 1.1 \cdot P_{\text{thr}}$ (a) and $P_{\text{in}} = 5 \cdot P_{\text{thr}}$ (b). The slope of the dashed line corresponds to the linewidth of the phonon laser.

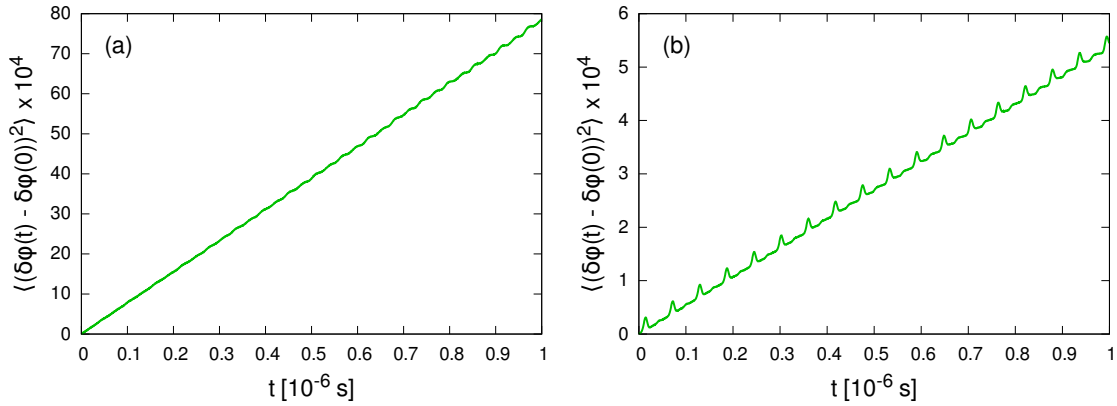


Figure 4.15: Phonon laser phase diffusion for the experimental parameter set with $\gamma_{\text{tip}} = 2\pi \cdot 30 \text{ MHz}$ for different pump powers $P_{\text{in}} = 1.1 \cdot P_{\text{thr}}$ (a) and $P_{\text{in}} = 5 \cdot P_{\text{thr}}$ (b).

While the oscillations become quite large at higher input powers for $\gamma_{\text{tip}} = 0$ (fig. 4.14), the effect is relatively small for $\gamma_{\text{tip}} = 2\pi \cdot 30 \text{ MHz}$ (fig. 4.15). In both cases, however, the average phase diffusion is still a linear function of time and the average slope of the curve represents the phonon laser linewidth.

As a first investigation of the phonon laser linewidth behavior, we calculated the dependence of the linewidth on the output power of the laser, the result of which is displayed in fig. 4.16. It turns out that the linewidth is a linear function of the inverse output power, $\Delta\omega \propto 1/P_{\text{out}}$. This is exactly the same behavior as it is the case for an optical laser (cf. eqs. (2.48) and (2.49)).

We now address the central question of this thesis concerning the phonon laser linewidth in the vicinity of an EP. Analogously to the procedure established in sections 4.1.2 and 4.1.3, we aim to calculate also the linewidth of the phonon laser as a function of γ_{tip} . However, the value of γ_{tip} influences not only the linewidth but also the output lasing power of the phonon laser. As already shown before, the linewidth linearly

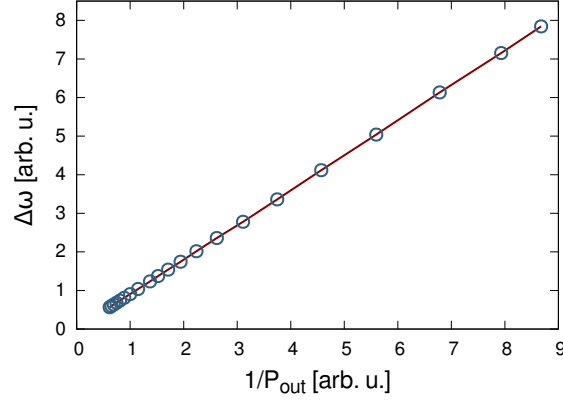


Figure 4.16: Phonon laser linewidth as a function of the inverse output power $1/P_{\text{out}}$.

depends on the inverse output power and therefore decreases when P_{out} is increased. In order to produce results which are comparable to each other, this effect has to be taken into account. For each given value of γ_{tip} , either the input power must always be chosen such that the output power is kept constant or the linewidth has to be normalized to the respective output power. For the affected calculations presented in this section, the latter method has been applied, i.e. each linewidth value was calculated with $P_{\text{in}} = 1.1 \cdot P_{\text{thr}}$ and normalized according to

$$\Delta\omega \rightarrow \Delta\omega \cdot \frac{P_{\text{out}}}{P_{\text{out}}^{\text{EP}}}, \quad (4.9)$$

where $P_{\text{out}}^{\text{EP}}$ is the value of P_{out} for $\gamma_{\text{tip}} = \gamma_{\text{tip}}^{\text{EP}}$ and $P_{\text{in}} = 1.1 \cdot P_{\text{thr}}$. Following this procedure, a remarkable behavior of the linewidth near the EP is revealed. Similar to the phonon laser threshold or the optomechanical amplification, the linewidth strongly depends on the driving frequency ω_{d} (see fig. 4.17). For $\omega_{\text{d}} = \omega_{\text{m}} + \omega_{\text{c}}$, the linewidth decreases monotonously with increasing γ_{tip} . In contrast, for $\omega_{\text{d}} = \omega_{\text{m}} + \omega_{\pm}$, the linewidth first increases and then decreases as a function of γ_{tip} with a maximum not directly at but close to the EP in the regime before the EP. This effect can be observed for the experimental as well as for the modified parameter set. In both cases, the maximum is more pronounced when $\omega_{\text{d}} = \omega_{\text{m}} + \omega_{+}$ is used. Nevertheless, the height of the maximum is much smaller for the experimental than for the modified parameter set. It is worth noting that as for the threshold or mechanical amplification results (see figs. 4.8 and 4.9), the linewidth curve has a kink at the position of the EP where also the driving frequency shows a kink.

The experimental results for the phonon laser linewidth behavior are presented in fig. 4.18. The output power dependence of the linewidth measured in the experiment agrees very well with the theoretical result shown in fig. 4.16. Furthermore, the linewidth broadening in the vicinity of the EP was also observed in the experiment. However, the height of the experimentally observed maximum clearly exceeds the calculated value (by a factor of 200). In addition, the maximum seems to appear directly at the EP, which is, however, hard to determine due to the small number of available data points.

To get additional insight into the phonon laser linewidth characteristics, several

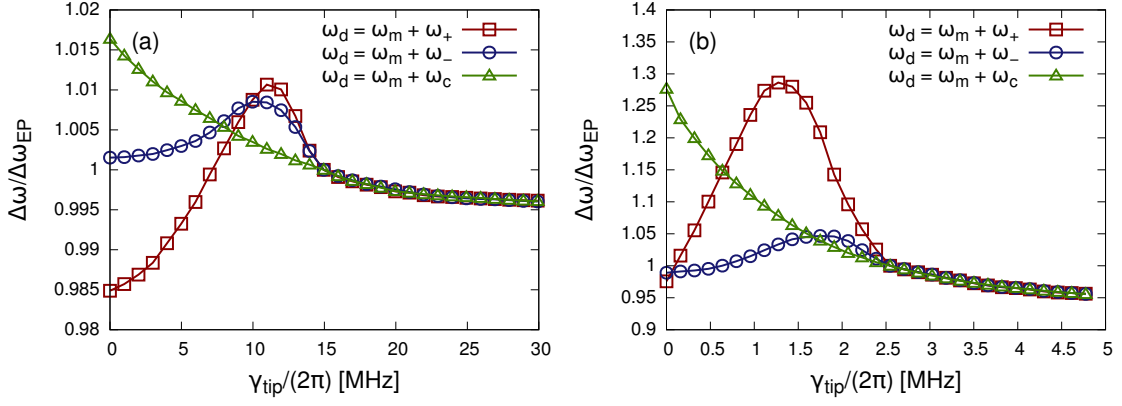


Figure 4.17: Phonon laser linewidth as a function of γ_{tip} , normalized to the linewidth value at the EP ($\Delta\omega_{EP}$). The curve is shown for both the experimental parameter set (a) and the modified parameter set (b) with three different driving frequencies ω_d .

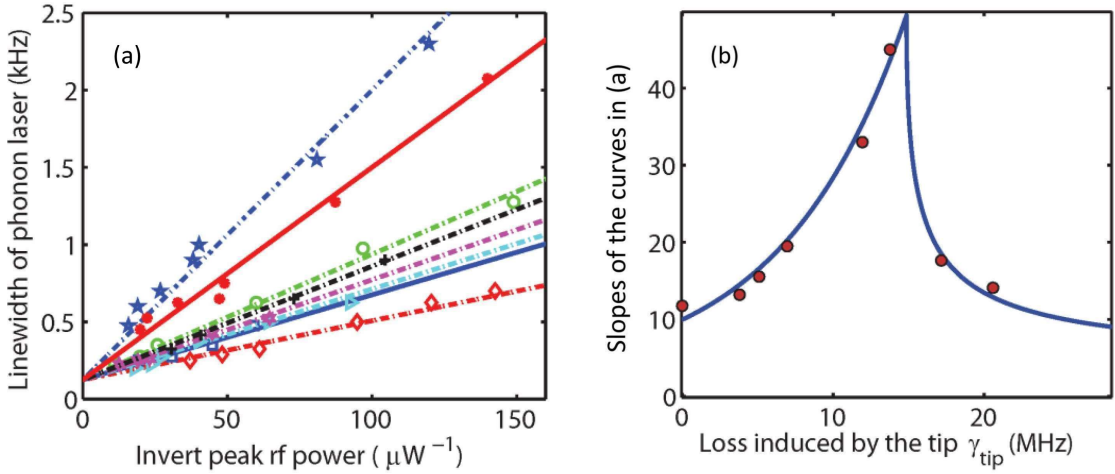


Figure 4.18: Experimental results for the phonon laser linewidth in the vicinity of an EP induced by the additional loss γ_{tip} . The left figure (a) shows the power dependence of the linewidth for different values of γ_{tip} . The right figure (b) shows the slopes of the curves in (a) as a function of γ_{tip} and can be understood as a cut through the curves in (a) for a fixed output power. Figure courtesy of Şahin Özdemir (*Washington University in St. Louis*).

calculations for different parameter sets have been performed¹⁰. The results suggest that the linewidth is qualitatively almost independent of the optomechanical coupling gx_0 (see fig. 4.19). For both experimental and modified parameter sets, the shape of the linewidth curve does not change when the value of gx_0 is varied by a factor of 10. Quantitatively, the results are only scaled by a constant factor because the signal-to-noise ratio is changed when gx_0 is varied (cf. fig. 4.4). Qualitatively different behaviors can be observed by varying the mechanical dissipation rate γ_m (see fig. 4.20). In this case,

¹⁰ These calculations were performed with the driving frequency $\omega_d = \omega_m + \omega_+$, which coincides with the procedure from the experiment.

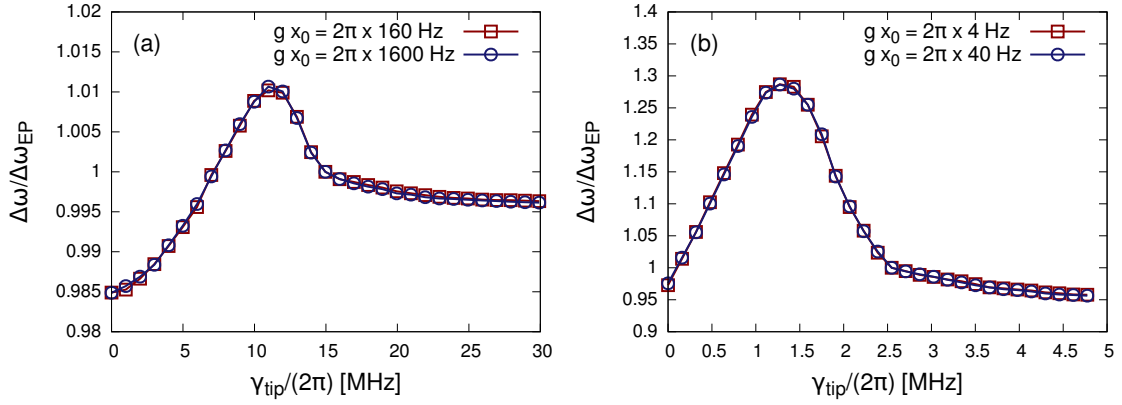


Figure 4.19: Phonon laser linewidth as a function of γ_{tip} , normalized to the linewidth value at the EP ($\Delta\omega_{EP}$). The curve is shown for both the experimental parameter set (a) and the modified parameter set (b) with two different optomechanical coupling rates $g x_0$.

the signal-to-noise ratio is also changed since the noise strength depends on the value of γ_m . However, varying that parameter also shows an effect on the qualitative linewidth behavior. For the experimental as well as for the modified parameter set, the linewidth broadening in the vicinity of the EP is enhanced when γ_m is increased. Moreover, the position of the maximum is slightly shifted and moved away from the EP for larger values of γ_m . Finally, the influence of the inter-resonator coupling strength κ is examined (see [fig. 4.21](#)). One finds that κ has an important influence on the phonon laser linewidth. On the one hand, the choice of κ determines the value of γ_{tip} where the EP occurs. This is the reason why the maximum in the linewidth curve is shifted when κ is varied. On the other hand, the supermode frequencies and therefore also the driving frequency strongly depend on κ . As already shown before, the driving frequency has a substantial influence on the linewidth. However, one can observe two qualitatively different behaviors of the linewidth for our two different parameter sets. For the experimental parameter set, the effect of the linewidth broadening near the EP is reduced for increasing κ while the modified parameter set features a growing linewidth enhancement for higher values of κ .

In summary, by using the parameter values that were provided by the experimentalists, the theoretical results for the linewidth behavior in the vicinity of the EP could not reproduce the experimental observations. However, it turned out that the correspondence between calculated and measured results can be improved by adjusting certain parameter values. As we have shown, a major influence factor for the linewidth is given by the inter-resonator coupling strength κ . The value of κ is controlled by the distance between the two optical cavities in our system. If the gap between the WGMRs is accidentally changed during a measurement, this modifies the coupling constant κ , which might be a possible explanation for the discrepancy between theory and experiment (cf. [section 4.1.3](#)). In addition, some of the system parameters are difficult to be determined precisely. Therefore, the parameter values can contain a significant error.

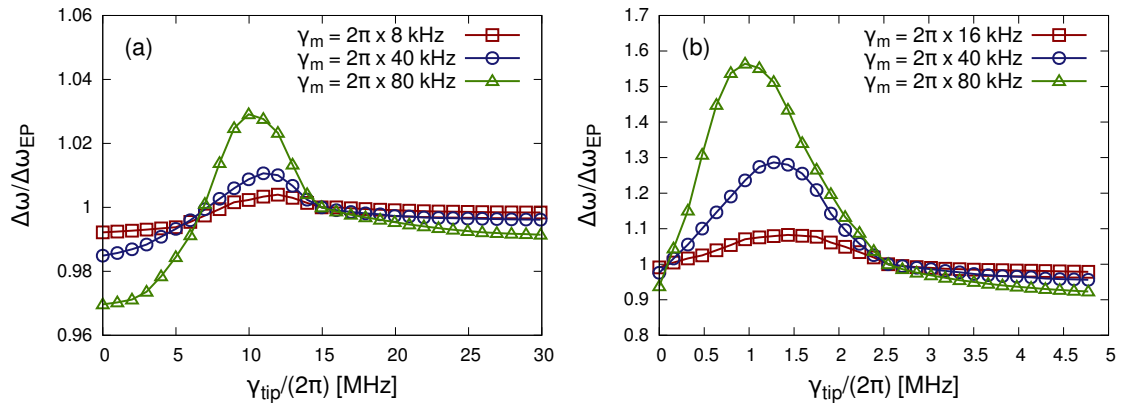


Figure 4.20: Phonon laser linewidth as a function of γ_{tip} , normalized to the linewidth value at the EP ($\Delta\omega_{EP}$). The curve is shown for both the experimental parameter set (a) and the modified parameter set (b) with three different mechanical dissipation rates γ_m .

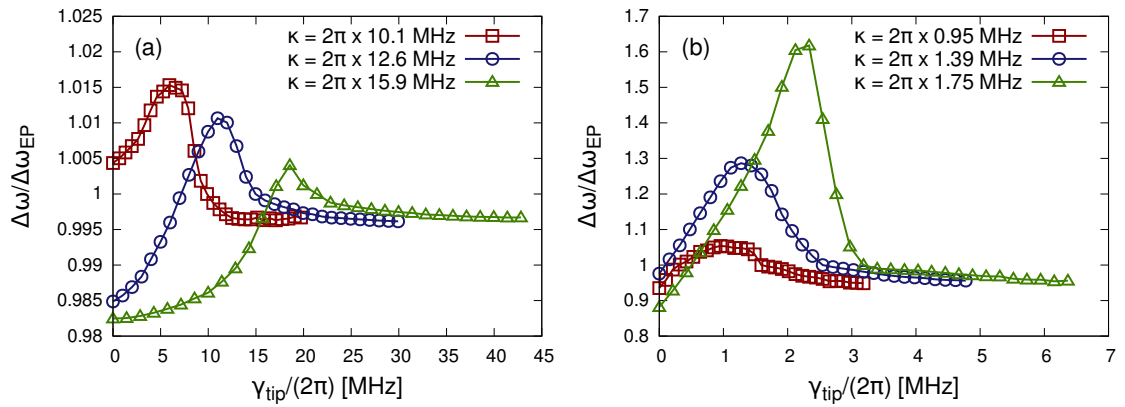


Figure 4.21: Phonon laser linewidth as a function of γ_{tip} , normalized to the linewidth value at the EP ($\Delta\omega_{EP}$). The curve is shown for both the experimental parameter set (a) and the modified parameter set (b) with three different inter-resonator coupling rates κ .

5 Conclusions and Outlook

The goal of this thesis was to establish the theory for a phonon laser system and to compare the theoretical results with the experimental ones provided by the *Micro/Nano Photonics Lab* at *Washington University in St. Louis*.

For this purpose, we have constructed a Hamiltonian (eq. (2.14)) and three corresponding Langevin equations (eqs. (2.30) to (2.32)) that describe the system used in the experiment. In this context, we have also found certain conditions that characterize the corresponding Langevin noise forces involving the diffusion coefficients eqs. (2.44) to (2.47). Furthermore, a method for solving stochastic differential equations was presented where we have developed a procedure to implement the noise such that all constraints for the diffusion coefficients are fulfilled (see section 3.1).

In the remaining part of the thesis, various calculations have been performed to investigate the properties of the phonon laser system. First, the characteristics of the solutions of the system equations were examined (section 4.1.1), where we showed the existence of a laser threshold. While the solutions for the fields are given by constant values below threshold, one can observe an oscillating behavior above threshold. Furthermore, the dependence of the threshold pump power as well as of the optomechanical amplification on the system parameters was explored (sections 4.1.2 and 4.1.3). In particular, we focused our study on the system behavior in the vicinity of an exceptional point (EP), which occurs if some of the eigenvalues and eigenmodes of a system coalesce (see section 2.3). It turned out that the results strongly depend on the driving frequency and one can observe a large variation of the quantities under investigation around the EP. These results, which were calculated without the influence of the noise, show rather good agreement with the experimental data. Finally, we have performed various calculations for the phonon laser linewidth by including the complete noise (section 4.2.2). The validity of our calculation method was checked in section 4.2.1. Similarly as for a conventional optical laser, the linewidth of the phonon laser is a linear function of the inverse output power. Additionally, it was shown that the variation of certain system parameters significantly influences the linewidth, especially in the vicinity of the EP. The qualitative linewidth behavior, however, is mainly governed by the choice of the driving frequency. On the one hand, if the driving frequency is chosen to be the sum of one of the optical supermode frequencies plus the mechanical resonance frequency, a broadening of the linewidth can be observed with a maximum near the EP. On the other hand, if the driving frequency is set to be equal to the constant value given by the sum of the optical cavity resonance frequency plus the mechanical resonance frequency, only a monotonous behavior around the EP can be observed. The effect of the linewidth broadening at the EP could also be observed in the experiment. In fact, this effect is much more pronounced in the experimental observations than in our theoretical calculations.

The experimental linewidth results could thus not be fully reproduced by our theory, which might be either an indication for a problem with the parameter values or for another missing link in the theoretical framework.

Since phonon lasers represent a relatively new area of research, there is still a lot of work that has to be done in the future. In order to obtain a larger number of comparative results, further experiments with different parameters would be desirable. In particular, it would be very helpful to investigate experimentally the effect of the driving frequency on the results to verify our theoretical observations. As the extent of the linewidth broadening in the experiment exceeded the theoretical prediction of this effect considerably, such additional measurements would help to clarify the differences between experiment and theory.

As a next step, the behavior of different phonon laser systems could be analyzed in detail. For instance, an interesting line of research would be to study the phonon laser characteristics for the case of \mathcal{PT} -symmetry, when both gain and loss are present in the system, as suggested in [55]. In such a situation, the occurrence of an EP is always accompanied by a symmetry-breaking transition whose effects on the system properties would be interesting to be examined. Such kind of investigations might contribute substantially to a deeper understanding of the phonon laser linewidth mechanism or to other aspects of the theoretical framework.

Generally, the usability of the phonon laser could be improved by deliberately controlling characteristic properties like the lasing frequency or intensity. The phonon laser is not yet at a stage to be directly used for technological applications, but if it undergoes a similar development as the optical laser, it may soon be an integral part of the technology we use on an everyday basis.

Acknowledgements

The completion of the present work would not have been possible without the help and support of many people whom I wish to thank at this point of my master thesis.

First of all, I want to express my special gratitude to my advisor, Prof. Stefan Rotter, whose patient guidance, enthusiastic encouragement, and immense knowledge have been a great help throughout the entire project. I appreciate that the door to his office was always open for discussions whenever I ran into difficulties or had a question about my research.

My profound thankfulness also goes to my second thesis advisor, Dmitry Krimer, who supported me with his scientific experience in many ways. I am very grateful for the countless hours he has spent on discussing theory and results, for reviewing my theoretical derivations and program source codes, and for providing a lot of beneficial critique about this thesis and my work in general.

Special thanks are extended to the group of Lan Yang from *Washington University in St. Louis* who have performed the experiments presented in this thesis. In particular, I want to thank Şahin Özdemir for welcoming us into this collaboration and for providing the experimental data as well as the information about the experimental setup.

I would like to thank Matthias Liertz for his help with various computer problems and other issues, as well as for many stimulating discussions of theoretical matters.

Additionally, I want to thank the colleagues from the third floor offices for many useful tips and tricks, pleasant conversations, and a lot of fun.

Finally, my sincere gratefulness is admitted to my family for their encouragement and support during my studies and throughout my whole life.

List of Figures and Tables

Fig. 2.1	Principle of stimulated emission	4
Fig. 2.2	Phonon laser system	5
Fig. 2.3	Eigenvalues of a non-Hermitian matrix	13
Fig. 2.4	Frequencies and dissipation rates of the supermodes	15
Fig. 3.1	Wiener process	18
Tab. 4.1	Phonon laser system parameters	27
Fig. 4.1	Time-dependent solution of the phonon laser system	29
Fig. 4.2	Time-dependent solution of the phonon laser system	30
Fig. 4.3	Transient of the numerical solution for the phonon mode	32
Fig. 4.4	Influence of the Langevin noise on the phonon laser field	33
Fig. 4.5	Phonon laser intensity as a function of the input pump power	34
Fig. 4.6	Experimental results for the phonon laser threshold for different values of the loss induced by the tip	34
Fig. 4.7	Comparison between theoretical and experimental results for the phonon laser threshold	35
Fig. 4.8	Phonon laser threshold as a function of the loss induced by the tip	35
Fig. 4.9	Phonon laser intensity as a function of the loss induced by the tip	36
Fig. 4.10	Experimental results for the phonon laser intensity for different values of the loss induced by the tip	36
Fig. 4.11	Phonon laser intensity as a function of the loss induced by the tip	37
Fig. 4.12	Influence of Langevin noise on a laser field	38
Fig. 4.13	Phase diffusion and linewidth	39
Fig. 4.14	Phonon laser phase diffusion	40
Fig. 4.15	Phonon laser phase diffusion	40
Fig. 4.16	Dependence of the phonon laser linewidth on the output power	41
Fig. 4.17	Phonon laser linewidth in the vicinity of an EP	42
Fig. 4.18	Experimental results for the phonon laser linewidth in the vicinity of an EP	42
Fig. 4.19	Phonon laser linewidth in the vicinity of an EP	43
Fig. 4.20	Phonon laser linewidth in the vicinity of an EP	44
Fig. 4.21	Phonon laser linewidth in the vicinity of an EP	44

Bibliography

- [1] C. E. Webb and J. D. C. Jones. *Handbook of Laser Technology and Applications*. Institute of Physics Publishing, Bristol (2004).
- [2] K. Jakubczak. *Lasers: Applications in Science and Industry*. InTech, Rijeka, Croatia (2011).
- [3] P. A. Fokker, J. I. Dijkhuis, and H. W. De Wijn. *Stimulated emission of phonons in an acoustical cavity*. *Physical Review B* **55**, 2925 (1997).
- [4] I. V. Volkov, S. T. Zavtrak, and I. S. Kuten. *Theory of sound amplification by stimulated emission of radiation with consideration for coagulation*. *Physical Review E* **56**, 1097 (1997).
- [5] A. J. Kent, R. N. Kini, N. M. Stanton, M. Henini, B. A. Glavin, V. A. Kochelap, and T. L. Linnik. *Acoustic Phonon Emission from a Weakly Coupled Superlattice under Vertical Electron Transport: Observation of Phonon Resonance*. *Physical Review Letters* **96**, 215504 (2006).
- [6] K. Vahala, M. Herrmann, S. Knünz, V. Batteiger, G. Saathoff, T. W. Hänsch, and T. Udem. *A phonon laser*. *Nature Physics* **5**, 682 (2009).
- [7] R. P. Beardsley, A. V. Akimov, M. Henini, and A. J. Kent. *Coherent terahertz sound amplification and spectral line narrowing in a stark ladder superlattice*. *Physical Review Letters* **104**, 085501 (2010).
- [8] I. S. Grudinin, H. Lee, O. Painter, and K. J. Vahala. *Phonon laser action in a tunable two-level system*. *Physical Review Letters* **104**, 083901 (2010).
- [9] H. Haken. *Laser Theory*. Springer, Berlin (1983).
- [10] H. Haken. *Light: Volume II: Laser Light Dynamics*. North Holland, Amsterdam (1985).
- [11] M. Liertzer, L. Ge, A. Cerjan, A. D. Stone, H. E. Türeci, and S. Rotter. *Pump-induced exceptional points in lasers*. *Physical Review Letters* **108**, 173901 (2012).
- [12] M. Brandstetter, M. Liertzer, C. Deutsch, P. Klang, J. Schöberl, H. E. Türeci, G. Strasser, K. Unterrainer, and S. Rotter. *Reversing the pump dependence of a laser at an exceptional point*. *Nature Communications* **5** (2014).

- [13] B. Peng, Ş. K. Özdemir, S. Rotter, H. Yilmaz, M. Liertzer, F. Monifi, C. M. Bender, F. Nori, and L. Yang. *Loss-induced suppression and revival of lasing*. Science **346**, 328 (2014).
- [14] A. Einstein. *Strahlungs-Emission und -Absorption nach der Quantentheorie*. Deutsche Physikalische Gesellschaft **18** (1916).
- [15] J. Kabuss, A. Carmele, T. Brandes, and A. Knorr. *Optically driven quantum dots as source of coherent cavity phonons: a proposal for a phonon laser scheme*. Physical Review Letters **109**, 054301 (2012).
- [16] J. Kabuss, A. Carmele, and A. Knorr. *Threshold behavior and operating regimes of an optically driven phonon laser: Semiclassical theory*. Physical Review B **88**, 064305 (2013).
- [17] M. Aspelmeyer, T. J. Kippenberg, and F. Marquardt. *Cavity optomechanics*. Reviews of Modern Physics **86**, 1391 (2014).
- [18] C. V. Raman and K. S. Krishnan. *A new type of secondary radiation*. Nature **121**, 501 (1928).
- [19] G. Landsberg. *Eine neue Erscheinung bei der Lichtzerstreuung in Krystallen*. Naturwissenschaften **16**, 558 (1928).
- [20] L. Yong-Chun, H. Yu-Wen, W. C. Wei, and X. Yun-Feng. *Review of cavity optomechanical cooling*. Chinese Physics B **22**, 114213 (2013).
- [21] V. B. Braginsky, M. L. Gorodetsky, and V. S. Ilchenko. *Quality-factor and nonlinear properties of optical whispering-gallery modes*. Physics Letters A **137**, 393 (1989).
- [22] A. Schliesser and T. J. Kippenberg. *Cavity optomechanics with whispering-gallery mode optical micro-resonators*. Advances in Atomic, Molecular, and Optical Physics **58**, 207 (2010).
- [23] K. Hill, B. Kawasaki, and D. Johnson. *Low-threshold cw Raman laser*. Applied Physics Letters **29**, 181 (1976).
- [24] C. K. Law. *Interaction between a moving mirror and radiation pressure: A Hamiltonian formulation*. Physical Review A **51**, 2537 (1995).
- [25] C. W. Gardiner and M. J. Collett. *Input and output in damped quantum systems: Quantum stochastic differential equations and the master equation*. Physical Review A **31**, 3761 (1985).
- [26] C. W. Gardiner and P. Zoller. *Quantum Noise: A Handbook of Markovian and Non-Markovian Quantum Stochastic Methods with Applications to Quantum Optics*. Springer, Berlin (2004).

-
- [27] M. O. Scully and M. S. Zubairy. *Quantum Optics*. Cambridge University Press, Cambridge (1997).
- [28] L. Davidovich. *Sub-Poissonian processes in quantum optics*. Reviews of Modern Physics **68**, 127 (1996).
- [29] A. L. Schawlow and C. H. Townes. *Infrared and Optical Masers*. Physical Review **112**, 1940 (1958).
- [30] S. J. M. Kuppens, M. P. Van Exter, and J. P. Woerdman. *Quantum-Limited Linewidth of a Bad-Cavity Laser*. Physical Review Letters **72**, 3815 (1994).
- [31] S. J. M. Kuppens, M. A. Van Eijkelenborg, C. A. Schrama, M. P. Van Exter, and J. P. Woerdman. *Incomplete Inversion and Double-Valued Fundamental Linewidth of Infrared HeNe and HeXe Lasers*. IEEE Journal of Quantum Electronics **32**, 383 (1996).
- [32] C. Henry. *Theory of the Linewidth of Semiconductor Lasers*. IEEE Journal of Quantum Electronics **18**, 259 (1982).
- [33] K. Petermann. *Calculated spontaneous emission factor for double-heterostructure injection lasers with gain-induced waveguiding*. IEEE Journal of Quantum Electronics **15**, 566 (1979).
- [34] A. E. Siegman. *Excess spontaneous emission in non-Hermitian optical systems. I. Laser amplifiers*. Physical Review A **39**, 1253 (1989).
- [35] A. E. Siegman. *Excess spontaneous emission in non-Hermitian optical systems. II. Laser oscillators*. Physical Review A **39**, 1264 (1989).
- [36] G. H. C. New. *The origin of excess noise*. Journal of Modern Optics **42**, 799 (1995).
- [37] W. A. Hamel and J. P. Woerdman. *Observation of enhanced fundamental linewidth of a laser due to nonorthogonality of its longitudinal eigenmodes*. Physical Review Letters **64**, 1506 (1990).
- [38] M. A. Van Eijkelenborg, Å. M. Lindberg, M. S. Thijssen, and J. P. Woerdman. *Resonance of quantum noise in an unstable cavity laser*. Physical Review Letters **77**, 4314 (1996).
- [39] Y. D. Chong and A. D. Stone. *General linewidth formula for steady-state multimode lasing in arbitrary cavities*. Physical Review Letters **109**, 063902 (2012).
- [40] A. Pick, A. Cerjan, D. Liu, A. W. Rodriguez, A. D. Stone, Y. D. Chong, and S. G. Johnson. *Ab initio multimode linewidth theory for arbitrary inhomogeneous laser cavities*. Physical Review A **91**, 063806 (2015).

- [41] A. Cerjan, A. Pick, Y. D. Chong, S. G. Johnson, and A. D. Stone. *Quantitative test of general theories of the intrinsic laser linewidth*. Optics Express **23**, 28316 (2015).
- [42] H. E. Türeci, A. D. Stone, and B. Collier. *Self-consistent multimode lasing theory for complex or random lasing media*. Physical Review A **74**, 043822 (2006).
- [43] L. Ge, Y. D. Chong, and A. D. Stone. *Steady-state ab initio laser theory: Generalizations and analytic results*. Physical Review A **82**, 063824 (2010).
- [44] T. Kato. *Perturbation Theory for Linear Operators*. Springer, Berlin (1966).
- [45] M. V. Berry. *Physics of nonhermitian degeneracies*. Czechoslovak Journal of Physics **54**, 1039 (2004).
- [46] W. D. Heiss. *Exceptional points of non-Hermitian operators*. Journal of Physics A: Mathematical and General **37**, 2455 (2004).
- [47] W. D. Heiss. *The physics of exceptional points*. Journal of Physics A: Mathematical and Theoretical **45**, 444016 (2012).
- [48] T. J. Milburn, J. Doppler, C. A. Holmes, S. Portolan, S. Rotter, and P. Rabl. *General description of quasiadiabatic dynamical phenomena near exceptional points*. Physical Review A **92**, 052124 (2015).
- [49] J. Doppler, A. A. Mailybaev, J. Böhm, U. Kuhl, A. Girschik, F. Libisch, T. J. Milburn, P. Rabl, N. Moiseyev, and S. Rotter. *Dynamically encircling exceptional points in a waveguide: asymmetric mode switching from the breakdown of adiabaticity*. arXiv preprint arXiv:1603.02325 (2016).
- [50] H. Eleuch and I. Rotter. *Exceptional points in open and PT symmetric systems*. arXiv preprint arXiv:1311.6320 (2013).
- [51] C. M. Bender and S. Boettcher. *Real spectra in non-Hermitian Hamiltonians having \mathcal{PT} symmetry*. Physical Review Letters **80**, 5243 (1998).
- [52] K. G. Makris, R. El-Ganainy, D. N. Christodoulides, and Z. H. Musslimani. *Beam Dynamics in \mathcal{PT} Symmetric Optical Lattices*. Physical Review Letters **100**, 103904 (2008).
- [53] C. E. Rüter, K. G. Makris, R. El-Ganainy, D. N. Christodoulides, M. Segev, and D. Kip. *Observation of parity–time symmetry in optics*. Nature Physics **6**, 192 (2010).
- [54] B. Peng, Ş. K. Özdemir, F. Lei, F. Monifi, M. Gianfreda, G. L. Long, S. Fan, F. Nori, C. M. Bender, and L. Yang. *Parity-time-symmetric whispering-gallery microcavities*. Nature Physics **10**, 394 (2014).

- [55] H. Jing, Ş. K. Özdemir, X.-Y. Lü, J. Zhang, L. Yang, and F. Nori. *\mathcal{PT} -symmetric phonon laser*. *Physical Review Letters* **113**, 053604 (2014).
- [56] M. V. Berry. *Mode degeneracies and the Petermann excess-noise factor for unstable lasers*. *Journal of Modern Optics* **50**, 63 (2003).
- [57] C. W. Gardiner. *Handbook of Stochastic Methods: for Physics, Chemistry and the Natural Sciences*. Springer, Berlin (2002).
- [58] R. Toral and P. Colet. *Stochastic Numerical Methods: An Introduction for Students and Scientists*. Wiley-VCH, Weinheim (2014).
- [59] W. H. Press. *Numerical Recipes: The Art of Scientific Computing*. Cambridge University Press, Cambridge (2007).
- [60] P. Glendinning. *Stability, Instability and Chaos: An Introduction to the Theory of Nonlinear Differential Equations*. Cambridge University Press, Cambridge (1994).